



Effects of Patch–Matrix Composition and Individual Movement Response on Population Persistence at the Patch Level

James T. Cronin¹ · Jerome Goddard II²  · Ratnasingham Shivaji³

Received: 24 October 2017 / Accepted: 19 June 2019
© Society for Mathematical Biology 2019

Abstract

Fragmentation creates landscape-level spatial heterogeneity which in turn influences population dynamics of the resident species. This often leads to declines in abundance of the species due to increased susceptibility to edge effects between the remnant habitat patches and the lower quality “matrix” surrounding these focal patches. In this paper, we formalize a framework to facilitate the connection between small-scale movement and patch-level predictions of persistence through a mechanistic model based on reaction–diffusion equations. The model is capable of incorporating essential information about edge-mediated effects such as patch preference, movement behavior, and matrix-induced mortality. We mathematically analyze the model’s predictions of persistence with a general logistic-type growth term and explore their sensitivity to demographic attributes in both the patch and matrix, as well as patch size and geometry. Also, we provide bounds on demographic attributes and patch size in order for the model to predict persistence of a species in a given patch based on assumptions on the patch/matrix interface. Finally, we illustrate the utility of this framework with a well-studied planthopper species (*Prokelisia crocea*) living in a highly fragmented landscape. Using experimentally derived data from various sources to parameterize the model, we show that, qualitatively, the model results are in accord with experimental predictions regarding minimum patch size of *P. crocea*. Through application of a sensitivity analysis to the model, we also suggest a ranking of the most important model parameters based on which parameter will cause the largest output variance.

Keywords Minimum patch size · Reaction diffusion equations · Habitat fragmentation · Matrix effects

Mathematics Subject Classification 92D40 · 35J25

This material is based upon work supported by the National Science Foundation under Grant Nos. DMS-1516519, DMS-1516833, and DMS-1516560.

Extended author information available on the last page of the article

1 Introduction

1.1 Background and Motivation

Human activities over the past centuries have greatly exacerbated the fragmentation of habitats [e.g., Heilman et al. (2002), Ewers et al. (2013), Uchida and Ushimaru (2014)]. This fragmentation creates landscape-level spatial heterogeneity which in turn influences the population dynamics of the resident species. Of particular concern, it often leads to declines in abundance of the species due to increased susceptibility to edge effects between the remnant habitat patches and the lower quality human-modified “matrix” surrounding these focal patches (Ries et al. 2004; Fagan et al. 1999; Cantrell et al. 1998). In a comprehensive synthesis of empirical and theoretical evidence of edge effects, Fagan et al. coined the term “edge-mediated effects” to denote the mechanisms through which edges alter ecological processes (Fagan et al. 1999). Two edge-mediated effects that are of fundamental importance in the study of habitat fragmentation on a single species at the patch level are: (1) the alteration of how individuals move and (2) the alteration of mortality in response to edges.

Although studies of movement behavior in response to different habitat edge conditions are relatively scarce, these studies clearly demonstrate that the composition of the matrix can influence emigration rates, patterns of movement and within-patch distributions of a species [e.g., Tschardt et al. (2002), Schooley and Wiens (2004), Haynes and Cronin (2006)]. Even in the same fragmented habitat, movement behavior has been shown to be very species specific (Reeve and Cronin 2010). With regard to alteration of mortality at patch edges, Cantrell et al. (1998) argued that matrix types with increased mortality risk may threaten species with extinction as habitat patches are “drained” of their occupants. The empirical examples cited in Cantrell and Cosner (1999), that illustrate the detrimental patch-level effects of increased matrix hostility, were linked to human activities that altered matrix composition (e.g., housing development and mortality from domesticated pets).

Connecting the wealth of empirical information available about individual movement and mortality in response to matrix composition to predictions about patch-level persistence is indeed a formidable task for which there is no coherent framework available (Maciel and Lutscher 2013). The reaction diffusion framework and its underlying random walk models have been widely used by ecologists (Turchin 1998; Cantrell and Cosner 2003; Holmes et al. 1994), and their great strength is that the model’s dynamics can be analyzed mathematically, providing important patch-level predictions of population persistence. The reaction diffusion framework is also ideally suited to handle fragmentation and edge-mediated effects as the partial differential equation(s) involved require explicit definition of edge behavior via boundary conditions (Cantrell and Cosner 2003; Fagan et al. 1999).

In the now classical paper of Ludwig et al. (1979), the authors addressed a long-standing problem in ecology and conservation biology—the minimum patch size for population persistence. Here, they assumed a one-dimensional patch is surrounded by a “sea” of hostile territory (matrix), the patch edge is invisible to organisms, and the matrix did not necessarily inflict immediate mortality. Cantrell and Cosner (1998)

also modeled edge-mediated movement behavior in a one-dimensional patch model but without matrix effects by employing skew Brownian motion. However, skew Brownian motion has the undesirable property that habitat edges can serve as sources or sinks for the population (Maciel and Lutscher 2013). More recently, Ovaskainen and Cornell (2003) modified the random walk formulation to include movement behavior based on habitat preference at patch edges. The random walk formulation gave rise to interface conditions between spatial patches of varying quality. Maciel and Lutscher (2013) later generalized the work of Ovaskainen and Cornell (2003) to integrate movement behavior and patch preference into the classical reaction diffusion framework. They consider persistence and spread of a species in a one-dimensional infinite periodic landscape consisting of alternating “favorable” and “unfavorable” patches. Maciel and Lutscher (2013) concluded that predictions of persistence varied widely among three different patch–matrix interface scenarios when the matrix diffusion rate was allowed to vary, whereas predictions were consistent across all three interfaces with respect to changing matrix death rate and habitat preference.

In the present article, we formalize a framework built upon the random walk models of these previous authors to simultaneously explore the effects of changes in movement behavior at an edge, patch preference, and matrix hostility on predictions of persistence for a one-, two-, or even three-dimensional patch with sufficiently smooth boundary. We then mathematically analyze these predictions of persistence with a general logistic-type growth term and explore their sensitivity to demographic attributes in the matrix (diffusion rate and death rate), patch preference, demographic attributes in the patch (intrinsic growth rate and diffusion rate), and patch size. The methods employed give far more global results for predictions of persistence than the methods used in Maciel and Lutscher (2013). In particular, we confirm the predictions of persistence given in Maciel and Lutscher (2013) and extend them to a general patch in 1, 2, and 3 dimensions and any reasonable shape (with sufficiently smooth boundary) and for a class of reaction terms that are characteristically logistic in nature, thus making their predictions more robust. As a test and example of the application of the model framework, we use it to predict the minimum patch size for the planthopper, *P. crocea* living in patches surrounded by two matrix types known to greatly affect their movement and edge behavior (Haynes and Cronin 2006; Reeve et al. 2008). Empirical estimates for all parameters in the model are available for this species as well as some information on the relationship between patch size and population persistence.

1.2 Modeling Framework

The reaction diffusion framework is based on individual movement assumptions described by a random walk. In this case, it is assumed that both movement and reproduction occur locally and on the same time scale (see Okubo (1980), Cantrell and Cosner (2003), Holmes et al. (1994), for example). In order to separate the combined effects of patch size and patch geometry on population persistence, we consider a patch Ω_0 to be a bounded, connected, open subset of \mathbb{R}^n when $n = 1, 2$, or 3 with $|\Omega_0| = 1$, where

$$|\Omega_0| = \begin{cases} \text{length of } \Omega_0; & n = 1 \\ \text{area of } \Omega_0; & n = 2 \\ \text{volume of } \Omega_0; & n = 3. \end{cases}$$

We assume here that the boundary of Ω_0 (denoted by $\partial\Omega_0$) is smooth. Now, we define the focal patch as $\Omega = \{\ell x \mid x \in \Omega_0\}$ yielding:

$$|\Omega| = \begin{cases} \ell; & n = 1 \\ \ell^2; & n = 2 \\ \ell^3; & n = 3, \end{cases}$$

where ℓ is a positive parameter representing the patch size [(see Cantrell and Cosner (2003)]. In the model, $u(t, x)$ represents the density of a theoretical population inhabiting Ω . Here, the variable t represents time and x represents spatial location within Ω . The model is then:

$$\begin{aligned} u_t &= D\Delta u + ruf(u); \quad t > 0, x \in \Omega \\ u(0, x) &= u_0(x); \quad x \in \Omega \\ D \frac{\partial u}{\partial \eta} + \frac{\sqrt{S_0 D_0}}{\kappa} u &= 0; \quad t > 0, x \in \partial\Omega \end{aligned} \tag{1}$$

where the parameter D is the diffusion rate inside the patch, D_0 is the diffusion rate in the matrix surrounding Ω , r is the patch intrinsic growth rate, S_0 is the death rate in the matrix, and κ is a parameter encapsulating assumptions regarding the patch/matrix interface such as patch preference and movement behavior. Also, $\frac{\partial u}{\partial \eta}$ represents the outward normal derivative of u , $rf(u)$ is the per-capita growth rate of the population inside Ω , and u_0 is the initial distribution of population density in the patch. The parameters D , D_0 , S_0 , r , and κ are always positive. Note that the derivation of the boundary condition in (1) is discussed in Sect. 2.1. We will be concerned with growth terms that are characteristically logistic and as such satisfy:

- (F1) There exists a $K > 0$ such that $f(u) > 0$ for $u \in [0, K)$, $f(K) = 0$, and $f(u) < 0$ for $u > K$;
- (F2) $f'(u) < 0$ for $u \geq 0$.

Here, the parameter K represents the carrying capacity inside the patch. For example, the typical logistic per-capita growth rate of $f(u) = (1 - \frac{u}{K})$ satisfies (F1) and (F2) with a carrying capacity of K . For convenience, we choose $f(0) = 1$, since otherwise we could just scale r and K to make $f(0) = 1$. We note that the theta-logistic per-capita growth rate (see Sibly et al. (2005), for example) satisfies (F1)–(F2) and thus will be covered in our analysis.

2 Mathematical Modeling and Interpretation

2.1 Derivation of the Boundary Condition in (1)

Here, we discuss the derivation of the boundary condition found in (1) via a combination of the approaches of Maciel and Lutscher (2013) and Cantrell et al. (1998) under the patch/matrix interface conditions given in these respective papers. Additionally, we explore the interface scenarios suggested in Maciel and Lutscher (2013) and Cantrell and Cosner (2007) and introduce a standard scaling argument to reduce the problem to a more tractable single reaction diffusion model.

The boundary condition in (1) allows modeling of the effects of movement behavior changes in response to patch/matrix interface and hostility of the matrix surrounding the patch. To see this, combine the approach of modeling the effects of an unsuitable matrix in Ludwig et al. (1979) with the interface conditions given in Maciel and Lutscher (2013) for a one-dimensional patch $\Omega = (0, \ell)$ ($\ell > 0$ denotes the patch size) surrounded by an infinite “sea” of hostile territory. Following the derivation in Ludwig et al. (1979), exterior to Ω , the population density w is subject to the growth law:

$$w_t = D_0 w_{xx} - S_0 w \quad (2)$$

where D_0 is a positive parameter representing the diffusion rate and S_0 is a positive parameter representing the death rate of the organism in the matrix. As in Maciel and Lutscher (2013), making the assumption of continuity of flux is a natural condition that will imply all organisms leaving the patch will enter the matrix and organisms leaving the matrix will enter the patch. In other words, no organisms are introduced or lost at the interface. However, a discontinuity arises in the density at the patch/matrix interface which accounts for changes in movement behavior. To formalize this, letting D be the diffusion rate inside Ω and following the random walk derivation given in Maciel and Lutscher (2013) the interface conditions become:

$$D \frac{\partial u}{\partial \eta} = D_0 \frac{\partial w}{\partial \eta_0}; \quad x \in \{0, \ell\} \quad (3)$$

$$u = \kappa w; \quad x \in \{0, \ell\} \quad (4)$$

where κ is a positive, unitless parameter whose exact form depends on movement behavior assumptions as we will explain later, η is the outward normal direction for the patch, and η_0 is the inward normal direction for the matrix. We now make the assumption that the population density is at a stationary state in the matrix which from (2) must be of the form $w(x) = C_1 e^{\sqrt{\frac{S_0}{D_0}}x}$ for $x \leq 0$ and similarly for $x \geq \ell$. Applying (3) and (4) will immediately yield the boundary condition in (1).

For patches in higher dimensions with arbitrary boundary shapes, easily extending such a derivation is not possible. With this one-dimensional boundary condition derivation in mind, we make the assumption that the population density is at a stationary state in the matrix whose distribution is approximated by exponential decay at a

rate of $\sqrt{\frac{S_0}{D_0}}$ away from the patch. The boundary condition in (1) is then a reasonable approximation of the true boundary behavior of the organism, where the parameter S_0 can be interpreted as a death rate in the matrix, D_0 as the diffusion rate in the matrix, and κ as a measure of the discontinuous “jump” in density at the patch/matrix interface. In Sect. 6.1, we provide a comparison of the accuracy of the model to predict minimum patch size for a two-dimensional disk, square, and proper rectangle (see also “Appendix C” where we provide a derivation of a mechanistically correct (at least in terms of steady states and their stability) model for the special case of a disk-shaped patch in two dimensions, namely (36)). Based upon our numerical exploration, we conjecture that this assumption should provide a reasonable approximation to the correct mechanistic formulation for patches that are simply connected and convex.

2.2 Patch–Matrix Interface Scenarios and Scaling

We now describe the interface scenarios suggested in Maciel and Lutscher (2013) and Cantrell and Cosner (2007). Recall that in the random walk model, organisms are assumed to move the step size Δx with probability p every Δt units of time. The diffusion rate is then obtained by taking parabolic limits in such a way that

$$D = \lim_{\Delta x, \Delta t \rightarrow 0^+} \frac{p \Delta x^2}{\Delta t} \quad (5)$$

is finite and positive (Okubo 1980; Turchin 1998; Cantrell and Cosner 2003). We now list four possible scenarios in Table 1 along with their κ -value, name, biological interpretation, and selected references for each scenario. In what follows, α will denote the probability that an organism remains in the patch upon reaching the patch/matrix interface. Derivations of each scenario can be found in the references listed in the table. We note that a fourth type of discontinuous density (DD) is possible in that both the step sizes and movement probabilities differ between the patch and matrix. However, its derivation yields a κ -value that is simply proportional to the one in a Type I DD. Qualitatively, we do not expect a difference in model output in this fourth case versus Type I DD. Therefore, this case is omitted from our analysis. We also note that the assumptions made in continuous density (CD) and Type III DD imply that the patch diffusion rate (D) and matrix diffusion rate (D_0) must be same. However, previous authors have considered similar models with a CD or Type III DD interface assumption but allowed $D \neq D_0$ [see Maciel and Lutscher (2013)]. In fact, Maciel and Lutscher (2013) showed that under a CD interface assumption, a model prediction of diffusion-independent persistence is possible when $D \neq D_0$. In the analysis that follows, we will always consider the case that $D = D_0$ in both the CD and Type III DD cases.

We now introduce a standard scaling,

$$\tilde{x} = \frac{x}{\ell} \quad \& \quad \tilde{t} = rt. \quad (6)$$

Table 1 Listing of interface scenarios with descriptions and selected references

Scenario name	Scenario description	κ	References
Continuous density	Organisms move between the patch and matrix with equal probability. Step sizes and movement probabilities are equal in the patch and matrix	1	Ludwig et al. (1979)
Type I discontinuous density (DD)	Organisms modify their movement behavior at the patch/matrix interface and would have a probability α of remaining in Ω which may be different from 50%. Step sizes differ between the patch and matrix, whereas movement probabilities are equal	$\frac{\alpha}{1-\alpha} \sqrt{\frac{D_0}{D}}$	Ovaskainen and Cornell (2003), Maciel and Lutscher (2013)
Type II discontinuous density (DD)	Organisms modify their movement behavior at the patch/matrix interface and would have a probability α of remaining in Ω which may be different from 50%. Step sizes are equal between the patch and matrix, but movement probabilities are different	$\frac{\alpha}{1-\alpha} \frac{D_0}{D}$	Ovaskainen and Cornell (2003), Maciel and Lutscher (2013)
Type III discontinuous density (DD)	Organisms remain in Ω with probability α which may be different from 50%. Movement probabilities and step sizes are same between the patch and matrix	$\frac{\alpha}{1-\alpha}$	Cantrell and Cosner (1999, 2007)

It is easy to see that after applying this scaling and dropping the tilde, (1) becomes

$$\begin{aligned}
 u_t &= \frac{1}{\lambda} \Delta u + uf(u); \quad t > 0, x \in \Omega_0 \\
 u(0, x) &= u_0(x); \quad x \in \Omega_0 \\
 \frac{\partial u}{\partial \eta} + \frac{\ell \sqrt{S_0 D_0}}{\kappa D} u &= 0; \quad t > 0, x \in \partial \Omega_0
 \end{aligned} \tag{7}$$

where $\lambda = \frac{r \ell^2}{D}$ is unitless and $|\Omega_0| = 1$. With regard to habitat fragmentation, we are particularly interested in the predictions of persistence for the population given by (7) as the patch size varies for a fixed patch geometry. Additionally, it is of interest to explore how the predictions of persistence change as the patch demographic attributes, such as the intrinsic growth rate and diffusion rate, vary. In Table 2, we enumerate the different possibilities for the boundary condition of (7) as the different scenarios and patch attributes are changed for a fixed patch geometry. Although the patch geometry is seemingly fixed in this analysis, its effects are still included in the model’s predictions. In particular, we want to study how persistence depends on each of the parameters r , D , or ℓ for fixed values of the remaining parameters. To this end, we write the multiparameter model (7) in such a way as to ensure that the original parameters are split into two unitless composite parameters, namely λ and γ , in such a way that the parameter in question (r , D , or ℓ) occurs only in λ . This process gives several different forms of the boundary condition in (7) as listed in Table 2. We note that since $D = D_0$

Table 2 Boundary condition possibilities for (7)

Parameter of interest	Type I and Type III DD	Type II DD
r : intrinsic growth rate	$\kappa = \frac{\alpha}{1-\alpha} \sqrt{\frac{D_0}{D}}$ $\frac{\partial u}{\partial \eta} + \gamma u = 0; x \in \partial \Omega_0$	$\kappa = \frac{\alpha}{1-\alpha} \frac{D_0}{D}$ $\frac{\partial u}{\partial \eta} + \gamma u = 0; x \in \partial \Omega_0$
D : patch diffusion rate	$\gamma = \frac{1-\alpha}{\alpha} \frac{\ell \sqrt{S_0}}{\sqrt{D}}$ $\frac{\partial u}{\partial \eta} + \sqrt{\lambda} \gamma u = 0; x \in \partial \Omega_0$	$\gamma = \frac{1-\alpha}{\alpha} \frac{\ell \sqrt{S_0}}{\sqrt{D_0}}$ $\frac{\partial u}{\partial \eta} + \gamma u = 0; x \in \partial \Omega_0$
ℓ : patch size	$\gamma = \frac{1-\alpha}{\alpha} \frac{\sqrt{S_0}}{\sqrt{r}}$ $\frac{\partial u}{\partial \eta} + \sqrt{\lambda} \gamma u = 0; x \in \partial \Omega_0$	$\gamma = \frac{1-\alpha}{\alpha} \frac{\sqrt{S_0}}{\sqrt{D_0}}$ $\frac{\partial u}{\partial \eta} + \sqrt{\lambda} \gamma u = 0; x \in \partial \Omega_0$

Note that the continuous density scenario is a special case of Type III DD with $\alpha = \frac{1}{2}$, where DD denotes discontinuous density as described in Table 1

in CD and Type III DD interface scenarios, the boundary conditions for these two cases are almost identical to that of Type I DD. Thus, it suffices to only analyze Type I DD and Type II DD interface scenarios. In fact, the CD scenario can be considered as a special case of Type III DD in which $\alpha = \frac{1}{2}$ and Type III DD considered a special case of Type I DD in which $D = D_0$.

Thus, all twelve parameters of interest and interface condition pairs can be treated mathematically via study of the differential equation in (7) and one of the following boundary conditions:

$$\frac{\partial u}{\partial \eta} + \gamma u = 0; t > 0, x \in \partial \Omega_0 \tag{8}$$

$$\frac{\partial u}{\partial \eta} + \sqrt{\lambda} \gamma u = 0; t > 0, x \in \partial \Omega_0 \tag{9}$$

or written more conveniently as

$$\frac{\partial u}{\partial \eta} + \lambda^\mu \gamma u = 0; t > 0, x \in \partial \Omega_0 \tag{10}$$

where $\mu = 0$ and $\frac{1}{2}$ correspond to (8) and (9), respectively. Study of the multiparameter problem:

$$\begin{aligned}
 u_t &= \frac{1}{\lambda} \Delta u + u f(u); t > 0, x \in \Omega_0 \\
 u(0, x) &= u_0(x); x \in \Omega_0 \\
 \frac{\partial u}{\partial \eta} + \lambda^\mu \gamma u &= 0; t > 0, x \in \partial \Omega_0
 \end{aligned}
 \tag{11}$$

will cover all the forms listed in Table 2, where the meaning of the unitless parameter γ will depend on the parameter of interest and interface type. Note that this framework can be extended to model density-dependent boundary behavior simply by considering a density-dependent $\alpha = \alpha(u)$ and ultimately $\gamma = \gamma(u)$.

In the case of the continuous density scenario, organisms do not detect the change between the patch and matrix. Thus, they freely cross the boundary of the patch having a probability of remaining in the patch of 50% and without adjusting their movement behavior in the matrix. In this scenario, the difference between patch and matrix may be subtle to the organism and not cause a change in movement behavior (Haynes and Cronin 2006; Reeve et al. 2008). Notwithstanding, an organism operating under the assumptions of Type III DD would be able to detect the change between patch and matrix. However, in this scenario, the organism is only able to adjust its probability of remaining in the patch. Movement behavior (step length and movement probability) would be the same in the matrix versus the patch.

An organism operating under the assumptions of Type I DD would detect the edge of the patch and bias its movement at the edge choosing to stay in the patch with a probability other than 50%. In addition, the organism would alter the length of each step of its movements while maintaining the same movement probability. As an example, an organism may detect a harsh matrix, lower its probability of moving into the matrix, and then for those organisms actually leaving the patch, increase the length taken at each step in order to improve its chances of re-entering the patch or finding a new one.

Under the assumptions of Type II DD, an organism would again detect the edge of the patch and bias its movement at the edge, deciding to stay in the patch with a probability other than 50%. The organism would keep its step length equal in the patch and matrix but would alter the movement probability.

3 Mathematical Preliminaries

The dynamics of a reaction diffusion model such as (11) are almost completely determined by its steady states, i.e., solutions of

$$\begin{aligned} -\Delta u &= \lambda u f(u); \quad x \in \Omega_0 \\ \frac{\partial u}{\partial \eta} + \lambda^\mu \gamma u &= 0; \quad x \in \partial\Omega_0 \end{aligned} \quad (12)$$

(see Cantrell and Cosner (2003) for example). Thus, understanding the structure and stability properties of positive solutions of (12) will completely characterize the dynamics of (11) and allow descriptions of the relationship between the model's parameters and predictions of persistence for the theoretical population.

Given a solution of (12), u , its local stability properties can be determined by examining the sign of the principal eigenvalue, $\sigma_1 = \sigma_1(\Omega_0, \lambda, \gamma, \mu, u)$, of the linearized eigenvalue problem associated with (12):

$$\begin{aligned} -\Delta \phi - \lambda [f(u) + u f'(u)] \phi &= \sigma \phi; \quad x \in \Omega_0 \\ \frac{\partial \phi}{\partial \eta} + \lambda^\mu \gamma \phi &= 0; \quad x \in \partial\Omega_0 \end{aligned} \quad (13)$$

with corresponding eigenfunction, ϕ , which can be chosen such that $\phi > 0$; $x \in \overline{\Omega}_0$ and $\|\phi\|_\infty = 1$.

As with other models of the same type as (11), the principle of “invasion implies persistence” holds. In other words, if an organism is able to survive in Ω at low densities (and thus invade Ω), then the population will be able to persist in Ω . For the model (11), persistence can be determined by studying the stability of the trivial steady state, $u \equiv 0$, via consideration of the sign of $\sigma_1(\Omega_0, \lambda, \gamma, \mu, 0)$. Although this type of linearized stability can only determine the dynamics of the model locally near a steady state, much more can be shown in the case of a reaction term satisfying the logistic-type assumptions, (F1) and (F2). The following theorem allows an exact description of the global dynamics of (11) based solely on the sign of $\sigma_1(\Omega_0, \lambda, \gamma, \mu, 0)$.

Theorem 1 *Suppose that $f(u)$ satisfies (F1) and (F2). Let $\sigma_1(\Omega_0, \lambda, \gamma, \mu, 0)$ be the principal eigenvalue of (13) with corresponding eigenfunction, ϕ , chosen such that $\phi > 0$; $x \in \overline{\Omega}_0$ and $\|\phi\|_\infty = 1$. Then, we have the following:*

- (a) *If $\sigma_1(\Omega_0, \lambda, \gamma, \mu, 0) \leq 0$, then (11) has no positive equilibrium and $u(t, x)$ will tend to the stable trivial steady state, $u \equiv 0$, with exponential speed for any nonnegative initial density profile.*
- (b) *If $\sigma_1(\Omega_0, \lambda, \gamma, \mu, 0) > 0$, then the trivial steady state, $u \equiv 0$, is unstable, there exists a unique globally asymptotically stable positive steady state, u , to (11), and $u(t, x)$ will tend to this positive steady state as $t \rightarrow \infty$ for any positive initial density profile. Moreover, $\epsilon\phi < u < 1$ for $x \in \overline{\Omega}_0$ and $\epsilon > 0$ and small enough.*

The proof of Theorem 1 can be found in Propositions 3.1–3.3 in Cantrell and Cosner (2003).

In the following subsections, we will explicitly describe the relationship between a given parameter of interest (r , D , or ℓ) and the persistence of the population under each of the four interface scenarios given in Table 1. To accomplish this, we compare the linearized eigenvalue problem for the trivial steady state, (13), with the eigenvalue problem:

$$\begin{aligned} -\Delta\phi &= \Lambda\phi; \quad x \in \Omega_0 \\ \frac{\partial\phi}{\partial\eta} + \beta\phi &= 0; \quad x \in \partial\Omega_0, \end{aligned} \tag{14}$$

where $\beta \geq 0$ and we note that the Λ in (14) is the eigenvalue parameter. The fact that (14) has a principal eigenvalue $\lambda_1 = \lambda_1(\Omega_0, \beta) \geq 0$ and corresponding eigenfunction ϕ which can be chosen such that $\phi > 0$; $x \in \overline{\Omega}_0$ and $\|\phi\|_\infty = 1$ is classical (see Cantrell and Cosner (2003), for example). Lemma 1 in “Appendix B” lists several useful properties of $\lambda_1(\Omega_0, \beta)$. Now, comparing the eigenvalue problems (13) and (14), uniqueness of the principal eigenvalue implies that:

$$\lambda_1(\Omega_0, \beta) = \sigma_1(\Omega_0, \lambda, \gamma, \mu, 0) + \lambda \tag{15}$$

$$\beta = \lambda^\mu \gamma. \tag{16}$$

4 Mathematical Analysis of (11)

In this section, we will analyze the model (11) in each of the cases dictated by the parameter of interest.

4.1 Case 1: $\mu = 0$

Since $\mu = 0$, (11) becomes:

$$\begin{aligned} u_t &= \frac{1}{\lambda} \Delta u + uf(u); \quad t > 0, x \in \Omega_0 \\ u(0, x) &= u_0(x); \quad x \in \Omega_0 \\ \frac{\partial u}{\partial \eta} + \gamma u &= 0; \quad t > 0, x \in \partial\Omega_0 \end{aligned} \tag{17}$$

where the definition of γ depends on which interface scenario is assumed from Table 2. The dynamics of (17) are already well known [see Cantrell and Cosner (2003)]. For completeness and the ability to provide comparisons between the cases of μ , we briefly summarize the mathematical analysis of (17) in this subsection. It is easy to see that when $\mu = 0$, (15) and (16) yield:

$$\sigma_1(\Omega_0, \lambda, \gamma, 0, 0) = \lambda_1(\Omega_0, \gamma) - \lambda. \tag{18}$$

From Lemma 1 in ‘‘Appendix B,’’ we know that $\lambda_1(\Omega_0, 0) = 0$, $\lambda_1(\Omega_0, \gamma)$ is strictly increasing in γ , and $\lambda_1(\Omega_0, \gamma) \rightarrow \lambda_1^0(\Omega_0)$ (the principal eigenvalue of Laplace’s equation with Dirichlet boundary conditions) as $\gamma \rightarrow \infty$ giving rise to the following theorem.

Theorem 2 *Let $\lambda_1^*(\Omega_0, \gamma) = \lambda_1(\Omega_0, \gamma)$. Then, we have the following:*

- (a) $\sigma_1(\Omega_0, \lambda, \gamma, 0, 0) \geq 0$ if and only if $\gamma > 0$ and $\lambda \leq \lambda_1^*(\Omega_0, \gamma)$
- (b) $\sigma_1(\Omega_0, \lambda, \gamma, 0, 0) < 0$ if and only if either $\gamma = 0$ and $\lambda > 0$ or $\gamma > 0$ and $\lambda > \lambda_1^*(\Omega_0, \gamma)$

Thus, for any $\gamma > 0$ there will be a unique minimum λ -value, $\lambda_1^*(\Omega_0, \gamma)$, for which the model’s only steady state will be the globally asymptotically stable trivial state for $\lambda \leq \lambda_1^*(\Omega_0, \gamma)$ and for $\lambda > \lambda_1^*(\Omega_0, \gamma)$ the model will have a unique globally asymptotically stable positive steady state accompanied by the unstable trivial state.

4.2 Case 2: $\mu = \frac{1}{2}$

In this case, (11) becomes:

$$\begin{aligned} u_t &= \frac{1}{\lambda} \Delta u + uf(u); \quad t > 0, x \in \Omega_0 \\ u(0, x) &= u_0(x); \quad x \in \Omega_0 \\ \frac{\partial u}{\partial \eta} + \sqrt{\lambda} \gamma u &= 0; \quad t > 0, x \in \partial\Omega_0 \end{aligned} \tag{19}$$

where the definition of γ again depends on which interface scenario is chosen from Table 2. In this case, (15) and (16) become:

$$\sigma_1(\Omega_0, \lambda, \gamma, 0.5, 0) = \lambda_1(\Omega_0, \beta) - \lambda \tag{20}$$

$$\beta = \sqrt{\lambda}\gamma. \tag{21}$$

Solving for $\lambda = \frac{\beta^2}{\gamma^2}$ in (21) and then substituting λ into (20) gives

$$\sigma_1(\Omega_0, \lambda, \gamma, 0.5, 0) = \lambda_1(\Omega_0, \beta) - \frac{1}{\gamma^2}\beta^2. \tag{22}$$

Theorem 3 connects the sign of $\sigma_1(\Omega_0, \lambda, \gamma, 0.5, 0)$ to ranges of parameter space for λ and γ . Note that Fig. 1 illustrates Theorem 3.

Theorem 3 *Let $\gamma \geq 0$. Then, we have the following:*

- (a) *there exists a $\lambda_2^*(\Omega_0, \gamma) > 0$ such that*
 - (1) *if $\lambda \leq \lambda_2^*(\Omega_0, \gamma)$, then $\sigma_1(\Omega_0, \lambda, \gamma, 0.5, 0) \geq 0$*
 - (2) *if $\lambda > \lambda_2^*(\Omega_0, \gamma)$, then $\sigma_1(\Omega_0, \lambda, \gamma, 0.5, 0) < 0$.*
- (b) *$\lambda_2^*(\Omega_0, 0) = 0$, $(\lambda_2^*)_\gamma > 0$ for $\gamma > 0$, and $\lambda_2^*(\Omega_0, \gamma) \rightarrow \lambda_1^0(\Omega_0)$ as $\gamma \rightarrow \infty$.*

Proof of Theorem 3 Define $g(\beta) := \frac{1}{\gamma^2}\beta^2$ and let $\gamma > 0$. From Lemma 1, we again have that $\lambda_1(\Omega_0, 0) = 0$, $\lambda_1(\Omega_0, \beta)$ is a strictly increasing and concave function of β for $\beta > 0$, and $\lambda_1(\Omega_0, \beta) \rightarrow \lambda_1^0(\Omega_0)$ as $\beta \rightarrow \infty$. Also, from the proof of Lemma 1 given in ‘‘Appendix’’ and the fact that we can choose $\phi > 0$; $x \in \overline{\Omega_0}$, we have that $\lambda'_1(\Omega_0, 0) > 0$. To prove (a), note that $g(0) = 0$, $g'(0) = 0$ but $\lambda_1(\Omega_0, 0) = 0$, and $\lambda'_1(\Omega_0, 0) > 0$. Thus, $\lambda_1(\Omega_0, \beta) - \frac{1}{\gamma^2}\beta^2 > 0$ for $\beta > 0$ and small enough. But, since $\lambda_1(\Omega_0, \beta)$ is concave, strictly increasing, and bounded in β there exists a unique $\beta^*(\Omega_0, \gamma) > 0$ such that $\sigma_1(\Omega_0, \lambda, \gamma, 0.5, 0) = \lambda_1(\Omega_0, \beta) - \frac{1}{\gamma^2}\beta^2 \geq 0$ for $\beta \in [0, \beta^*(\Omega_0, \gamma)]$ and $\sigma_1(\Omega_0, \lambda, \gamma, 0.5, 0) = \lambda_1(\Omega_0, \beta) - \frac{1}{\gamma^2}\beta^2 < 0$ for $\beta > \beta^*(\Omega_0, \gamma)$ (see Fig. 1). Since $\lambda = \frac{\beta^2}{\gamma^2}$ and $\lambda_1(\Omega_0, 0) = 0$, the result immediately follows $\lambda_2^*(\Omega_0, \gamma) = \frac{[\beta^*(\Omega_0, \gamma)]^2}{\gamma^2}$. Part (b) is clear from Lemma 1 and the previous argument. □

Hence, for all $\gamma > 0$ then there will be a unique minimum λ -value, $\lambda_2^*(\Omega_0, \gamma)$, for which the model’s only steady state will be the globally asymptotically stable trivial state for $\lambda \leq \lambda_2^*(\Omega_0, \gamma)$ and for $\lambda > \lambda_2^*(\Omega_0, \gamma)$ the model will have a unique globally asymptotically stable positive steady state accompanied by the unstable trivial state.

5 Results

In this section, we discuss persistence of the organism with respect to each of the three cases of parameters of interest.

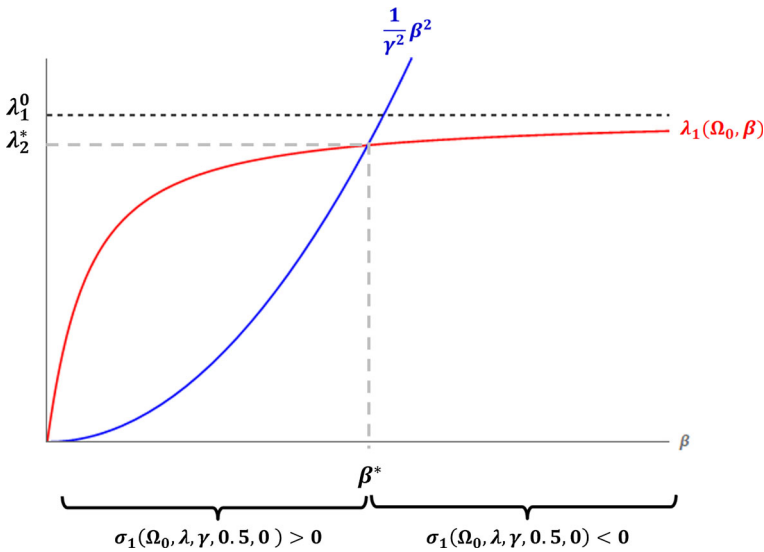


Fig. 1 Illustration of Theorem 3 (Color figure online)

5.1 Minimum Intrinsic Growth Rate for Persistence

Interpreting λ as being proportional to the intrinsic growth rate r means that study of (11) is equivalent to study of (17), regardless of the interface scenario assumption. From Theorem 2, given a $\gamma > 0$ will imply the existence of a minimum λ -value required for the population to persist, namely $\lambda_1^*(\Omega_0, \gamma)$. Note that in the case $\gamma = 0$, there is no such minimum λ -value since $\lambda_i^*(\Omega_0, 0) = 0, i = 1, 2$. From Table 2, $\gamma = 0$ if and only if either 1) $S_0 = 0$ meaning that matrix is not hostile or 2) $\alpha = 1$ (only in Type I–III DD) meaning that individuals that reach the patch boundary will never leave but always turn back into the patch. Both of these conditions will cause the boundary condition in (11) to become a repelling no-flux boundary condition. In this case, there is no loss of individuals through the boundary and the population can persist unconditionally. Thus, for what follows we will only consider the case when $\gamma > 0$. Using the definition of λ , we can then arrive at a corresponding minimum intrinsic growth rate required for a prediction of persistence for the theoretical population given a fixed patch diffusion rate and patch size:

$$r^*(\Omega_0, \gamma) = \frac{D\lambda_1^*(\Omega_0, \gamma)}{\ell^2}. \tag{23}$$

Using (23) and Theorem 2 yields the following result detailing the connection between the patch intrinsic growth rate and predictions of persistence from the model.

Corollary 1 *Let $\gamma > 0$ be defined as in Table 2 according to the interface scenario assumed. Then, we have the following:*

- (a) *if $r > r^*(\Omega_0, \gamma)$, then (11) has a unique positive equilibrium, u , that is a global attractor for nonnegative nontrivial solutions of (11);*

Table 3 Behavior of $r^*(\Omega_0, \gamma)$ under each of the four interface scenarios

	Type I and Type III DD	Type II DD
Behavior of r^* wrt α		$(r^*)_\alpha < 0; \alpha \in [0, 1]$ $r^* \rightarrow \frac{D\lambda_1^0(\Omega_0)}{\ell^2}$ as $\alpha \rightarrow 0^+$ $r^* \rightarrow 0$ as $\alpha \rightarrow 1^-$
Behavior of r^* wrt S_0		$(r^*)_{S_0} > 0; S_0 \geq 0$ $r^* \rightarrow 0$ as $S_0 \rightarrow 0^+$ $r^* \rightarrow \frac{D\lambda_1^0(\Omega_0)}{\ell^2}$ as $S_0 \rightarrow \infty$
Behavior of r^* wrt D_0	$(r^*)_{D_0} = 0; D_0 > 0$ no D_0 -dependence	$(r^*)_{D_0} < 0; D_0 > 0$ $r^* \rightarrow \frac{D\lambda_1^0(\Omega_0)}{\ell^2}$ as $D_0 \rightarrow 0^+$ $r^* \rightarrow 0$ as $D_0 \rightarrow \infty$

Note that the subscripts $\alpha, S_0,$ and D_0 denote partial derivatives and the continuous density scenario is a special case of Type III DD with $\alpha = \frac{1}{2}$

(b) if $r \leq r^*(\Omega_0, \gamma)$, then $u \equiv 0$ is a global attractor for nonnegative nontrivial solutions of (11).

Notice that this critical intrinsic growth rate r^* depends upon the geometry and size of Ω , the diffusion rate inside the patch D , and parameters implicit in the interface scenario assumption. Also from Theorem 2, it is easy to see that $r^*(\Omega_0, \gamma) \rightarrow \frac{D\lambda_1^0(\Omega_0)}{\ell^2}$ as $\gamma \rightarrow \infty$ giving rise to a maximal minimum intrinsic growth rate. Much more information can be obtained by studying the behavior of $r^*(\Omega_0, \gamma)$ as the interface parameters ($\alpha, S_0,$ and D_0) are allowed to vary for fixed patch size and patch diffusion rate. Table 3 lists the behavior of $r^*(\Omega_0, \gamma)$ under each of the interface scenarios.

Table 3 allows exploration of the relationship between minimum intrinsic growth rate and one-parameter-at-a-time (either $S_0, D_0,$ or α). To explore how this critical value varies as all relevant parameters ($D, \ell, S_0, D_0,$ and α) are allowed to change simultaneously, we employ a sensitivity analysis. Variance-based sensitivity analysis use is on the rise (Ferretti et al. 2016) since it provides global results for first-order interactions, higher-order interactions (e.g., the combined effect of two parameters changing simultaneously), and total effect index (an estimate of the total effect of a parameter including first and higher-order interactions) [see Saltelli et al. (2010), Saltelli et al. (2004), Saltelli et al. (2008)]. This type of sensitivity analysis typically makes use of Monte Carlo methods to estimate an ANOVA decomposition of the variance of a model across the entire parameter space (Saltelli et al. 2010).

Given a model with k parameters, variance-based sensitivity analysis typically results in k estimates of the first-order interaction and k estimates of total effect indices, both corresponding to the k parameters. For a detailed discussion of the ANOVA decomposition of variance of a model, see Saltelli et al. (2008). The model output in this sensitivity analysis is one of the three critical thresholds, either minimum intrinsic growth rate ($r^*(\Omega_0, \gamma)$), maximum diffusion rate ($D^*(\Omega_0, \gamma)$), or minimum patch size ($\ell^*(\Omega_0, \gamma)$). As seen in (23) (and similarly in the following subsections for $D^*(\Omega_0, \gamma)$)

Table 4 Sensitivity analysis results: minimum intrinsic growth rate in a disk-shaped patch

	ℓ	D	S_0	D_0	α
<i>Type I and Type III DD</i>					
Main effect (%)	14.1	0.0	0.0	0.0	0.0
Interaction effect (%)	80.0	2.7	1.5	0.0	59.6
Total effect (%)	94.1	2.7	1.5	0.0	59.6
<i>Type II DD</i>					
Main effect (%)	21.0	0.0	0.0	0.0	0.0
Interaction effect (%)	67.4	5.4	1.4	2.8	54.5
Total effect (%)	88.4	5.4	1.4	2.8	54.5
<i>Continuous density</i>					
Main effect (%)	85.0	0.0	0.0	0.0	0.0
Interaction effect (%)	13.8	7.3	9.0	0.0	0.0
Total effect (%)	98.8	7.3	9.0	0.0	0.0

Entries represent variance in $r^*(\Omega_0, \gamma)$

and $\ell^*(\Omega_0, \gamma)$) these critical values depend upon the principle eigenvalue of Laplace's equation with Robin boundary conditions via $\lambda_i^*(\Omega_0, \gamma)$, $i = 1, 2$, and thus need to be calculated numerically. To calculate these critical thresholds, we employed two functions in Mathematica (Wolfram Research Inc., version 11.3), (1) `NDEigensystem` to numerically estimate this principle eigenvalue for a given patch geometry and (2) `FindRoot` to numerically determine the value of $\lambda_i^*(\Omega_0, \gamma)$, $i = 1, 2$ (see Theorems 2 and 3).

The following parameters were selected on which to perform a variance-based sensitivity analysis depending on the model output: (1) minimum patch size: $x_1 = r$, $x_2 = D$, $x_3 = S_0$, $x_4 = D_0$, & $x_5 = \alpha$, (2) minimum intrinsic growth rate: $x_1 = \ell$, $x_2 = D$, $x_3 = S_0$, $x_4 = D_0$, & $x_5 = \alpha$, and maximum patch diffusion rate: $x_1 = r$, $x_2 = \ell$, $x_3 = S_0$, $x_4 = D_0$, & $x_5 = \alpha$. Applying sensitivity analysis to the model allows us to suggest a ranking of the most important model parameters based on which parameter will cause the largest output variance. This ranking could then be used to prioritize resources in an empirical study to ensure a greater degree of accuracy (which could be obtained, for example, via larger numbers of replicates for experiments designed to estimate model parameters). See "Appendix A" for a detailed description of the sensitivity analysis methodology. This sensitivity analysis performed on the minimum intrinsic growth rate for the case of the patch being a disk is represented in Table 4. Changing the patch geometry would more than likely change these results, though in this work we have not explored other geometries.

In Types I–III DD, the most important parameter is the patch size, followed by the probability of remaining in the patch upon reaching the patch/matrix interface and the patch diffusion rate. The matrix diffusion rate and death rate are close to tied for last. In the case of continuous density, the order is the same except for patch diffusion and matrix diffusion rates switch. For Types I–III DD, the majority of the total effect for patch size is due to higher-order interactions with the other parameters, while in continuous density scenarios main effects explain the majority of the total

effect. For this particular choice of parameter ranges, these results suggest that under any of the scenarios, if the true value of the patch size were provided, then the variance of the predictions of persistence could be reduced by 88–99%, depending on the scenario. In Types I & II DD, fixing the probability of leaving the patch upon reaching the patch/matrix interface to its true value would reduce the variation by around 55%. These sensitivity results indicate that for this choice of parameter ranges more resources should be committed to empirical estimation of patch size and probability of remaining in the patch upon reaching the patch/matrix interface (for Type I–III DD) than the remaining parameters in order to achieve a more accurate estimate for $r^*(\Omega_0, \gamma)$.

5.2 Maximum Patch Diffusion Rate for Persistence

Interpreting λ as being proportional to the reciprocal of the patch diffusion rate means that study of (11) is equivalent to study of (17) or (19), depending on the interface scenario assumption. Independent of the interface scenario assumption and for any $\gamma > 0$ the existence of a minimum λ -value required for the population to persist is guaranteed, namely $\lambda_i^*(\Omega_0, \gamma)$, where $i = 1$ or 2 depending on the interface scenario. Using the definition of λ , we can then arrive at corresponding maximum patch diffusion rates required for a prediction of persistence for the theoretical population given a fixed patch intrinsic growth rate and patch size:

$$D^*(\Omega_0, \gamma) = \begin{cases} \frac{r\ell^2}{\lambda_1^*(\Omega_0, \gamma)}; & \text{Type II DD} \\ \frac{r\ell^2}{\lambda_2^*(\Omega_0, \gamma)}; & \text{CD, Type I DD, or Type III DD} \end{cases} \tag{24}$$

Using (24) and Theorems 2 and 3 yields the following results detailing the connection between the patch diffusion rate and predictions of persistence from the model.

Corollary 2 *Let $\gamma > 0$ be defined as in Table 2 according to the individual interface scenario listed below. Then, we have the following:*

- (1) *if $D \geq D^*(\Omega_0, \gamma)$, then $u \equiv 0$ is a global attractor for nonnegative nontrivial solutions of (11);*
- (2) *if $D < D^*(\Omega_0, \gamma)$, then (11) has a unique positive equilibrium, u , that is a global attractor for nonnegative nontrivial solutions of (11);*

Notice that this critical patch diffusion rate D^* depends upon the geometry and size of Ω , the patch intrinsic growth rate r , and parameters implicit in the interface scenario assumption. As in the previous subsection, much more information can be obtained by studying the behavior of $D^*(\Omega_0, \gamma)$ as the interface parameters (α , S_0 , and D_0) are allowed to vary for fixed patch size and patch intrinsic growth rate. Table 5 lists the behavior of $D^*(\Omega_0, \gamma)$ under each of the interface scenarios.

Finally, a sensitivity analysis was performed on the maximum patch diffusion rate yielding Table 6. The sensitivity results again reveal a ranking of the most important parameters for the case of the patch being a disk and this particular choice of parameter ranges. In Type I & Type III DD, the most important parameter is the probability

Table 5 Behavior of $D^*(\Omega_0, \gamma)$ under each of the four interface scenarios

	Type I and Type III DD	Type II DD
Behavior of D^* wrt α	$(D^*)_\alpha > 0; \alpha \in [0, 1]$ $D^* \rightarrow \frac{r\ell^2}{\lambda_1^0(\Omega_0)}$ as $\alpha \rightarrow 0^+$ $D^* \rightarrow \infty$ as $\alpha \rightarrow 1^-$	
Behavior of D^* wrt S_0	$(D^*)_{S_0} < 0; S_0 \geq 0$ $D^* \rightarrow \infty$ as $S_0 \rightarrow 0^+$ $D^* \rightarrow \frac{r\ell^2}{\lambda_1^0(\Omega_0)}$ as $S_0 \rightarrow \infty$	
Behavior of D^* wrt D_0	$(D^*)_{D_0} = 0; D_0 > 0$ no D_0 -dependence	$(D^*)_{D_0} > 0; D_0 > 0$ $D^* \rightarrow \frac{r\ell^2}{\lambda_1^0(\Omega_0)}$ as $D_0 \rightarrow 0^+$ $D^* \rightarrow \infty$ as $D_0 \rightarrow \infty$

Note that the subscripts $\alpha, S_0,$ and D_0 denote partial derivatives and the continuous density scenario is a special case of Type III DD with $\alpha = \frac{1}{2}$

Table 6 Sensitivity analysis results: maximum patch diffusion rate in a disk-shaped patch

	ℓ	r	S_0	D_0	α
<i>Type I and Type III DD</i>					
Main effect (%)	0.1	0.1	1.0	0.0	5.1
Interaction effect (%)	73.4	62.3	60.8	0.0	93.2
Total effect (%)	73.6	62.4	61.8	0.0	98.3
<i>Type II DD</i>					
Main effect (%)	27.7	13.0	1.4	0.1	5.8
Interaction effect (%)	16.0	26.9	18.0	5.8	28.3
Total effect (%)	43.6	40.0	19.4	5.9	34.1
<i>Continuous density</i>					
Main effect (%)	0.3	0.0	17.7	0.0	0.0
Interaction effect (%)	17.6	20.5	44.3	0.0	0.0
Total effect (%)	17.9	20.5	62.0	0.0	0.0

Entries represent variance in $D^*(\Omega_0, \gamma)$

of remaining in the patch upon reaching the patch/matrix interface, followed by the patch size, and almost a tie for last in patch intrinsic growth rate and matrix death rate. Type II DD showed that the most important parameter was patch size, followed by patch intrinsic growth rate, probability of remaining in the patch upon reaching the patch/matrix interface, matrix death rate, and matrix diffusion rate. Finally, in the continuous density scenario, the ranking was matrix death rate, patch intrinsic growth rate, and patch size. In the Type II DD scenario, model output variance was mostly dominated by the main effects, whereas in the other scenarios it was dominated by higher-order interactions of the parameters. In each scenario, fixing the most important parameter at its true value can reduce variation in the model’s predictions by

anywhere from 44 to 98%. The stark differences in parameter importance suggested by the sensitivity analysis further corroborates the importance of the interface scenario assumption to the model’s predictions of persistence. These sensitivity results indicate that for this choice of parameter ranges more resources should be committed to empirical estimation of the parameter yielding the most model variance depending on interface scenario, in order to achieve a more accurate estimate for $D^*(\Omega_0, \gamma)$.

5.3 Minimum Patch Size Required for Persistence

Interpreting λ as being proportional to the patch size ℓ squared means that study of (11) is equivalent to study of (19), regardless of the interface scenario assumption. From Theorem 3, $\gamma > 0$ will always imply the existence of a minimum λ -value required for the population to persist, namely $\lambda_2^*(\Omega_0, \gamma)$. Using the definition of λ , we can then arrive at a corresponding minimum patch size required for a prediction of persistence for the theoretical population given a fixed patch diffusion rate and patch intrinsic growth rate:

$$\ell^*(\Omega_0, \gamma) = \sqrt{\frac{D}{r} \lambda_2^*(\Omega_0, \gamma)}. \tag{25}$$

Using (25) and Theorem 3 yields the following result detailing the connection between the patch size and predictions of persistence from the model.

Corollary 3 *Let $\gamma > 0$ be defined as in Table 2 according to the interface scenario assumed. Then, we have the following:*

- (a) *if $\ell > \ell^*(\Omega_0, \gamma)$, then (19) has a unique positive equilibrium, u , that is a global attractor for nonnegative nontrivial solutions of (19);*
- (b) *if $\ell \leq \ell^*(\Omega_0, \gamma)$, then $u \equiv 0$ is a global attractor for nonnegative nontrivial solutions of (19).*

Notice that this critical patch size ℓ^* depends upon the geometry of Ω_0 , the diffusion rate inside the patch D , patch intrinsic growth rate, and parameters implicit in the interface scenario assumption. Also from Theorem 3, it is easy to see that $\ell^*(\Omega_0, \gamma) \rightarrow \sqrt{\frac{D}{r} \lambda_1^0(\Omega_0)}$ as $\gamma \rightarrow \infty$ which gives rise to a maximal minimum patch size. Much more information can be obtained by studying the behavior of $\ell^*(\Omega_0, \gamma)$ as the interface parameters (α , S_0 , and D_0) are allowed to vary for fixed patch intrinsic growth rate and diffusion rate. Table 7 lists the behavior of $\ell^*(\Omega_0, \gamma)$ under each of the interface scenarios.

Finally, a sensitivity analysis was performed on the minimum patch size yielding Table 8. Sensitivity results again reveal a ranking of the most important parameters for the case of the patch being a disk and this particular choice of parameter ranges. In Type I–III DD and continuous density scenarios, the most important parameter is the patch intrinsic growth rate, followed by patch diffusion rate and the probability of remaining in the patch upon reaching the patch/matrix interface. The matrix diffusion rate and death rate are close to tied for last. For all scenarios, the majority of the total effect for patch intrinsic growth rate is due to main effects. In this case, there is very

Table 7 Behavior of $\ell^*(\Omega_0, \gamma)$ under each of the four interface scenarios

	Type I and Type III DD	Type II DD
Behavior of ℓ^* wrt α		$(\ell^*)_{\alpha} < 0; \alpha \in [0, 1]$ $\ell^* \rightarrow \sqrt{\frac{D}{r} \lambda_1^0(\Omega_0)}$ as $\alpha \rightarrow 0^+$ $\ell^* \rightarrow 0$ as $\alpha \rightarrow 1^-$
Behavior of ℓ^* wrt S_0		$(\ell^*)_{S_0} > 0; S_0 \geq 0$ $\ell^* \rightarrow 0$ as $S_0 \rightarrow 0^+$ $\ell^* \rightarrow \sqrt{\frac{D}{r} \lambda_1^0(\Omega_0)}$ as $S_0 \rightarrow \infty$
Behavior of ℓ^* wrt D_0	$(\ell^*)_{D_0} = 0; D_0 > 0$ no D_0 -dependence	$(\ell^*)_{D_0} < 0; D_0 > 0$ $\ell^* \rightarrow \sqrt{\frac{D}{r} \lambda_1^0(\Omega_0)}$ as $D_0 \rightarrow 0^+$ $\ell^* \rightarrow 0$ as $D_0 \rightarrow \infty$

Note that the subscripts α , S_0 , and D_0 denote partial derivatives and the continuous density scenario is a special case of Type III DD with $\alpha = \frac{1}{2}$

Table 8 Sensitivity analysis results: minimum patch size in a disk-shaped patch

	r	D	S_0	D_0	α
<i>Type I and Type III DD</i>					
Main effect (%)	79.0	3.7	0.6	0.0	6.0
Interaction effect (%)	12.6	11.9	0.8	0.0	5.2
Total effect (%)	91.6	15.6	1.4	0.0	11.2
<i>Type II DD</i>					
Main effect (%)	76.9	6.1	0.5	0.4	5.6
Interaction effect (%)	13.3	12.8	0.8	0.5	4.8
Total effect (%)	90.2	18.9	1.3	0.9	10.4
<i>Continuous density</i>					
Main effect (%)	85.2	3.6	1.0	0.0	0.0
Interaction effect (%)	12.8	10.8	0.4	0.0	0.0
Total effect (%)	98.0	14.4	1.4	0.0	0.0

Entries represent variance in $\ell^*(\Omega_0, \gamma)$

little variance due to interaction between the parameters. For this particular choice of parameter ranges, these results suggest that if the true value of the patch intrinsic growth rate were provided, then the variance of the predictions of persistence could be reduced by 90–98%, depending on the interface scenario assumptions, while fixing the patch diffusion rate to its true value would reduce the variation by around 14–19%. These sensitivity results indicate that for this choice of parameter ranges more resources should be committed to empirical estimation of intrinsic growth rate than the remaining parameters in order to achieve a more accurate estimate for $\ell^*(\Omega_0, \gamma)$.

5.4 Biological Interpretation

In each of the three parameters of interest cases, this analysis gives a minimum for patch intrinsic growth rate and patch size and a maximum for patch diffusion rate. In other words, for fixed values of the parameters, the patch (1) intrinsic growth rate, (2) diffusion rate, or (3) size must be large, small, or large enough, respectively, to overcome the loss of organisms through contact with the patch/matrix interface and hostility of the matrix or ensure that a sufficient proportion of the population avoids mortality induced through contact with the patch/matrix interface and hostility of the matrix. In the case of minimum patch size, this fact agrees with the well-known notion of a minimum core area (in the case of $n = 2$) requirement (Ohman and Eriksson 1998; Cronin 2009). The $\lambda_i^*(\Omega_0, \gamma)$ -values present in each of these bounds can be viewed as quantifying the loss of the population due to the unsuitable matrix where the i -value depends on the interface scenario assumed and γ encapsulates parameters regarding the interface. In particular, from (23)–(25) and the fact that the $\lambda_i^*(\Omega_0, \gamma)$'s are increasing functions of γ , increased matrix hostility yields higher γ -values which in turn yields more restrictive critical thresholds, e.g., larger minimum patch size. Note that these results are qualitatively similar to those in Skellam (1951).

The fact that $\lambda_i^*(\Omega_0, \gamma) \rightarrow \lambda_1^0(\Omega)$ as $\gamma \rightarrow \infty$ for each $i = 1$ or 2 , reveals a model prediction of the existence of a maximum possible effect of population loss due to the unsuitable matrix where this effect is quantified in $\lambda_1^0(\Omega)$. This phenomenon is well known in the case of minimum patch size [see, e.g., Cantrell and Cosner (2003)]. We also make note that this minimum patch size approaches infinity if either (1) the patch diffusion rate is arbitrarily large, since a large diffusion rate ensures that a very high proportion of the population will encounter loss at the patch/matrix interface, or (2) the intrinsic growth rate is arbitrarily small, which for a fixed patch diffusion rate will imply that the population is not able to recover the loss associated with interaction with unsuitable matrix. The maximum patch diffusion rate approaches zero (meaning no organism can colonize the patch) if either (1) the patch size is arbitrarily small, since a small patch ensures that a very high proportion of the population will encounter loss at the patch/matrix interface, or (2) the intrinsic growth rate is arbitrarily small. Finally, note that the minimum intrinsic growth rate approaches infinity if either (1) the patch diffusion rate is arbitrarily large or (2) the patch size is arbitrarily small. The complex definition of the maximum patch diffusion rate given in (24) and Corollary 2 reveals an important but somewhat subtle difference in exploring the predictions of persistence from the model (1) as the patch diffusion rate is varied for fixed values of the remaining parameters and for different interface scenario assumptions. This fact further increases the need to carefully identify the parameter of interest and interface scenario assumptions in order to correctly determine the model's predictions.

Tables 3, 5, and 7 give some insight into the behavior of the minimum intrinsic growth rate, maximum patch diffusion rate, and minimum patch size, respectively, as the interface parameters are varied. As expected in each of the parameters of interest, the continuous density scenario shows no α -dependence as the probability of remaining in the patch upon reaching the patch/matrix interface is fixed at 50%. The model further predicts that in Type I–III DD scenarios the minimum patch size and minimum intrinsic

growth rate are 0 when 100% of the population remain in the patch upon reaching the patch/matrix interface. In this case, the population is protected from the effects of the unsuitable matrix. Both minimum patch size and minimum intrinsic growth rates are monotonic decreasing functions of α . As this probability approaches 0%, more of the population is exposed to the effects of the unsuitable matrix and, in turn, the effect of population loss at the patch/matrix interface reaches its maximum value. As for maximum patch diffusion rate, the model predicts that in all scenarios this diffusion rate is ∞ when 100% of the population remain in the patch upon reaching the patch/matrix interface. The maximum patch diffusion rate is also a monotonic increasing function of α in Type I–III DD. As this probability approaches 0%, more of the population is exposed to the effects of the unsuitable matrix and, in turn, the effect of population loss at the patch/matrix interface reaches its maximum value. For all three parameters of interest under any of the interface scenarios, the population experiences no loss when the matrix death rate is 0 and the population experiences the maximum loss at the patch/matrix interface when the matrix death rate is arbitrarily large. Analysis of the model also reveals that minimum intrinsic growth rate and minimum patch size are monotonic increasing functions of the matrix death rate, while maximum patch diffusion rate is a monotonic decreasing function of matrix death rate.

Since the behaviors of all three parameters of interest with respect to the matrix diffusion rate are similar, we will only detail minimum patch size here. This behavior is starkly different depending on the interface scenario assumption. Type I DD, Type III DD, and CD scenarios all give a setting in which the minimum patch size is independent of the matrix diffusion rate. In Type I DD, the model assumes that organisms modify their behavior at the patch/matrix interface by showing different movement step sizes but the same movement probability between the patch and matrix. In this case, attempting to change the diffusion rate in the matrix would have no predicted benefit to the population's persistence. However, in the Type II DD scenario, it is assumed that organisms modify their movement behavior through altering their movement probability, while keeping their movement step size equal between the patch and matrix. These discrepancies between interface scenarios with respect to matrix diffusion rate are exactly the ones originally seen in Maciel and Lutscher (2013) for a one-dimensional patch. Our results extend their results to reasonable patches in one-, two-, or three-dimensional space (with sufficiently smooth boundary) and to more general logistic-type growth making them much more robust. In a sense, our results show that the mechanism behind these discrepancies is invariant with respect to domain geometry.

6 An Empirical Example and Numerical Exploration of the Accuracy of the Framework

In this section, we provide a partial numerical exploration of the framework's accuracy via comparison of minimum patch size estimates for the two-dimensional patch geometries: disk, square, and rectangle, and illustrate the utility of the framework via an empirical example. Due to the computationally expensive nature of this numerical

Table 9 Absolute error between $\ell^*(\Omega_0, \gamma)$ and $\ell^{**}(\Omega_0, \gamma_1, \gamma_2)$ with entries in parentheses representing error relative to the maximum minimum patch size

	Mean error	SD	Minimum error	Maximum error
Type I DD	0.21 (9.8%)	0.54 (14.1%)	2.82×10^{-6} ($1.2 \times 10^{-6}\%$)	7.35 (84.9%)
Type II DD	0.21 (9.3%)	0.54 (11.6%)	2.82×10^{-6} ($3.3 \times 10^{-6}\%$)	7.35 (60.6%)
Type III DD	0.24 (7.9%)	0.60 (9.6%)	2.82×10^{-6} ($9.7 \times 10^{-6}\%$)	7.35 (50.4%)
Continuous density	0.28 (9.5%)	0.63 (8.1%)	2.5×10^{-5} ($1.0 \times 10^{-5}\%$)	5.25 (26.7%)

exploration of the model, a more complete numerical exploration of the accuracy over parameter space is outside the scope of this current work.

6.1 Numerical Exploration of the Accuracy of the Framework

For the case of a disk in two dimensions, we provide a mechanically correct derivation of minimum patch size, $\ell^{**}(\Omega_0, \gamma_1, \gamma_2)$, in ‘‘Appendix C,’’ where γ_1, γ_2 are defined as in Table 13. We compared $\ell^*(\Omega_0, \gamma)$ to $\ell^{**}(\Omega_0, \gamma_1, \gamma_2)$ for 11, 973 parameter combinations, i.e., $(r, D_1, \alpha, D_0, S_0)$, where $r, D_1, D_0,$ & $S_0 \in [0.01, 10]$ and $\alpha \in [0, 1]$. Both absolute error and error relative to the maximum minimum patch size $\sqrt{\frac{r}{D_1} \lambda_1^0(\Omega_0)}$ for all 11, 973 parameter combinations are summarized in Table 9.

Comparison of the model (11) and the mechanically correct model for a two-dimensional disk (43) shows that $\ell^*(\Omega_0, \gamma) \approx \ell^{**}(\Omega_0, \gamma_1, \gamma_2)$ whenever $\gamma_2 \gg 1$, since $H(s) \approx 1$ for $s \gg 1$ (Yang and Chu 2016).

In the case of a rectangle in two dimensions, we employed a finite difference method (FDM) to numerically solve the time-dependent patch/matrix model (38) [see ‘‘Appendix C’’] with Ω being a rectangle with unit area centered at the origin and the region exterior to Ω , i.e., Ω_e , being the subset of the rectangle centered at the origin with an area of 10 not containing Ω . The boundary condition $w(t, x) \rightarrow 0; t > 0, |x| \rightarrow \infty$ was then replaced by $w(t, x) = 0; t > 0, |x| = 10$. Given a particular set of parameters for the model, i.e., $(r, D_1, \alpha, D_0, S_0)$, to numerically determine the minimum patch size for the system, a bisection method was employed on the interval of patch sizes, $\left[0, \sqrt{\frac{D_1}{r} \lambda_1^0(\Omega)}\right]$, with the right endpoint being the maximum minimum patch. The middle of the interval was then chosen as the patch size, i.e., $m = \frac{1}{2} \sqrt{\frac{D_1}{r} \lambda_1^0(\Omega)}$, and the initial density distribution was then taken as $w(0, x) = 0.0001; x \in \Omega$. The model was then run for several time steps to determine if $w(t, x)$ was increasing or decreasing. If the density decreased for a predetermined number of time steps, then that implied that m was below the true minimum patch size, and m lied above otherwise. The original interval was revised and the method continued until the bisection interval had length less than 0.05, say $[a, b]$. The maximum of the difference between a & b and $\ell^*(\Omega, \gamma)$ was then computed. Due to the computationally intensive nature of the method, r was fixed at 1, α fixed at 0.5, and only 170 parameter combinations, i.e., $(1, D_1, 0.5, D_0, S_0)$, were considered. The

Table 10 Absolute maximum error between $\ell^*(\Omega_i, \gamma)$ and the true minimum patch size with entries in parentheses representing error relative to the maximum minimum patch size

	Mean error	SD	Minimum error	Maximum error
<i>Ω_1 : a unit square</i>				
Type I DD	0.66 (8.6%)	0.33 (3.5%)	0.05 (1.2%)	1.74 (17.5%)
Type II DD	0.67 (8.5%)	0.38 (4.1%)	0.006 ($9.2 \times 10^{-4}\%$)	1.66 (16.7%)
<i>Ω_2 : a rectangle with lengths 2 and $\frac{1}{2}$</i>				
Type I DD	1.19 (10.5%)	0.70 (5.1%)	0.05 (0.6%)	3.50 (24.2%)
Type II DD	1.16 (10.2%)	0.62 (5.0%)	0.02 (0.2%)	2.75 (19.0%)
<i>Ω_3 : a rectangle with lengths 4 and $\frac{1}{4}$</i>				
Type I DD	3.41 (15.4%)	2.03 (7.7%)	0.06 (0.3%)	8.32 (29.5%)
Type II DD	3.33 (14.8%)	1.95 (7.5%)	0.03 (0.1%)	8.32 (29.5%)

absolute maximum error and error relative to the maximum minimum patch size for all 170 parameter combinations are summarized in Table 10 for Ω_1 a unit square, Ω_2 a rectangle with lengths 2 and $\frac{1}{2}$, and Ω_3 a rectangle with lengths 4 and $\frac{1}{4}$.

Overall, minimum patch size estimates using the model (11) had a mean relative error of 7.9–9.8% in the case of a disk and 8.5–15.4% in the case of a rectangle, with better accuracy coming from both disk and square. These numerical results indicate that accuracy of the minimum patch size estimate decreased as the patch became more elongated, as in the case of Ω_3 . In all cases of patch geometry, the accuracy of the minimum patch size estimate was linked to how well our assumption that the population density is at a stationary state in the matrix whose distribution is approximated by exponential decay at a rate of $\sqrt{\frac{S_0}{D_0}}$ away from the patch was satisfied. In other words, parameter values which provided the best estimate of true minimum patch size were exactly the ones whose matrix density at steady state was well approximated by exponential decay at a rate of $\sqrt{\frac{S_0}{D_0}}$ away from the patch. Although we did not explore the case of a nonconvex patch geometry, we conjecture that on the parts of the boundary where the outward normal direction would point toward another part of the patch, our exponential decay assumption would more than likely not be satisfied for any range of parameter values. Thus, the model would probably yield much less accurate predictions in that case than a convex patch geometry. These numerical results also indicate that the model's use in a particular experiential setup could be validated empirically via collection of density data in the matrix which could then be compared to our assumption of exponential decay at a rate of $\sqrt{\frac{S_0}{D_0}}$ away from the patch.

6.2 An Empirical Example: The Prairie Planthopper *Prokelisia crocea*

Predicting population persistence over a range of patch sizes, and estimating minimum patch size in response to changing landscape context, is an important goal in the field of landscape ecology (Fahrig 2001; Cronin and Reeve 2005, 2014) with clear applications to species conservation (Allen et al. 2001; Solomon et al. 2003). This model provides

Table 11 Parameter estimates for *P. crocea* [(from Haynes and Cronin (2006), Cronin (2007), Reeve et al. (2008)]

Parameter	Estimate
Diffusion	
Within cordgrass (brome matrix) (D)	0.1967 (0.1130, 0.3437) m ² /day
Within cordgrass (mudflat matrix) (D)	0.2956 (0.1773, 0.4933) m ² /day
Within brome (D_0)	0.1967 (0.1130, 0.3437) m ² /day
Within mudflat (D_0)	0.7669 (0.1882, 3.1245) m ² /day
Per-capita patch growth rate (r)	0.045 per day
Matrix death rate (same for brome and mudflat) (S_0)	0.36 per day
Probability of remaining in the patch (α)	
Brome	0.83 (0.704, 0.91)
Mudflat	0.976 (0.961, 0.986)

Numbers in parentheses are 95% confidence intervals

a framework for making these predictions, but there are relatively few species for which there are sufficient empirical data to estimate model parameters, particularly with regard to different landscape configurations (e.g., changing matrix composition). The planthopper *P. crocea* is one such exception. In addition to extensive data on the dispersal, boundary behavior and response to different matrix types, this is the only species to our knowledge for which there are also empirical data on the influence of matrix composition on population persistence—essential data for validating the model predictions.

P. crocea is a specialist herbivore of prairie cordgrass (*Spartina pectinata*) which grows in discrete clonal patches ranging in size from $< 1 \text{ m}^2$ to several hectares (Cronin 2003). The matrix within which these patches are embedded consists of three basic vegetation types: (1) periodically flooded mudflats, (2) mixtures of native grasses, and (3) monospecific stands of smooth brome (*Bromus inermis*) (Haynes and Cronin 2003). The latter matrix type is similar in stature and appearance to cordgrass, but the planthopper will not feed on it. Mark–release–recapture experiments have been conducted to quantify patterns of movement within cordgrass patches and in a mudflat or brome matrix and the redistribution of the planthopper in each of these habitats is well described by a diffusion model (Haynes and Cronin 2006; Reeve et al. 2008). In these same studies, the boundary behavior of the planthoppers was also quantified. Relevant parameter estimates from these experiments are reported in Table 11. Also included in the table is an estimate of the planthopper’s per-capita growth rate, r , derived from an experiment using caged planthoppers (from Cronin (2007)). Using a regression model to fit the relationship between the actual per-capita growth rate between successive generations and planthopper density, r was the estimated growth rate at zero density.

Observations made in the experiments performed in Haynes and Cronin (2006), Reeve et al. (2008) suggest that the Type III DD scenario best fits the planthopper when in patches surrounded by smooth brome. In particular, diffusion rates and step

lengths are similar within cordgrass and brome. In contrast, step lengths and diffusion rates are substantially greater in the more hostile mudflat matrix than in the cordgrass patches, best reflecting the Type I DD scenario. Also, when the matrix is mudflat, there is a much stronger bias toward staying in the patch (α) than when the matrix is brome.

In a corresponding landscape-scale experiment, Cronin et al. (2004), Cronin (2007) demonstrated that matrix composition could strongly influence planthopper persistence in a patch. Planthoppers released into experimentally created cordgrass patches (0.66 m^2) embedded in a mudflat matrix persisted for five generations, achieving relatively high and constant densities after the first generation [Fig. 2 in Cronin (2007)]. In contrast, planthoppers released into cordgrass patches in a brome matrix steadily declined and went extinct in all cases by the fifth generation. Although patch size was not explicitly considered in this experiment, the study suggests that the minimum patch size for planthoppers is $< 0.66 \text{ m}^2$ when the matrix is mudflat and $> 0.66 \text{ m}^2$ when the matrix is brome.

Using the model framework, and parameter estimates from Table 3, we generate predictions regarding the relationship between planthopper persistence and patch size for the three discontinuous density (DD) patch–matrix interface scenarios. The continuous density scenario, in which there is no boundary behavior or difference in movement behavior between matrix types, clearly does not apply to *P. crocea* and was omitted from this analysis. In this analysis, we allow the matrix to vary along a continuum in composition from pure mudflat (0% brome) to pure brome (100% brome). The two extremes mimic the experimental work described above, but, in nature, the matrix can be a mixture of the two and therefore it will be valuable to predict minimum patch sizes along this continuum. As a test of the validity of these models, we also compare these findings to the qualitative empirical conclusions about matrix composition (pure mudflat or pure brome) and estimates of minimum patch size from both (11) and the mechanistically correct model for a disk in two dimensions, (43) (see above). Finally, a sensitivity analysis is performed to evaluate which empirically derived parameter estimates have the greatest influence on predictions about the relationship between persistence and patch size. In choosing ranges of the parameters for the sensitivity analysis, we employed 95% confidence intervals for those parameters which we have them. For parameters without confidence intervals, we used the interval from 50% of the parameter estimate to 200% of the estimate.

A linear interpolation was employed for D , D_0 , α , and S_0 using the data points for 0% and 100% brome from Table 11. With these interpolations and the remaining parameter values from Table 11, a graph of brome percentage versus minimum patch size was generated using both the approximate model (11) and the mechanistically correct model for a disk in two dimensions (43) for both Type I DD and Type II DD scenarios in Fig. 2 (recall that Type III DD is only appropriate for the case of 100% brome when $D = D_0$). Based upon the experimental design of the patches, Ω was taken as a disk. For both scenarios, the minimum patch size increased as the percentage of brome in the matrix increased. The strongly reflecting boundary when matrix composition was predominantly mudflat (probability of remaining in the patch, $\alpha = 0.976$; Table 11) results in reduced losses of planthoppers from the patch, allowing population persistence in smaller patches. Under the Type I DD scenario, which best reflects planthopper movement and boundary behavior when the matrix is

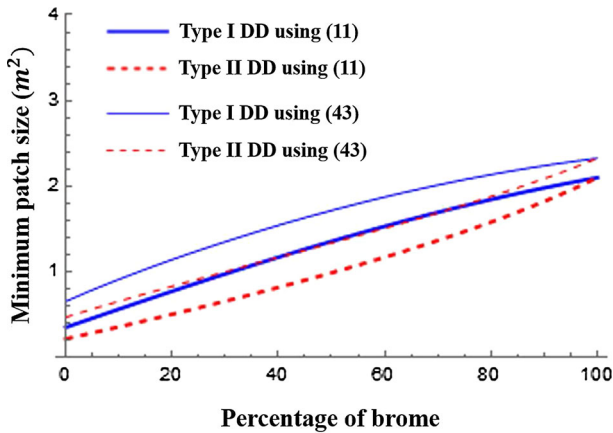


Fig. 2 The predicted relationship between matrix composition and minimum patch size for the planthopper, *P. crocea*. Separate curves are reported for each of the discontinuous patch–matrix interface scenarios, as well as for the models (11) and (43) (Color figure online)

pure mudflat (0% brome), the minimum patch size is estimated to be 0.35 m^2 using (11) and 0.65 m^2 using (43), whereas under the Type II DD scenario, the minimum patch size is estimated to be 0.22 m^2 using (11) and 0.47 m^2 using (43). In contrast, when the matrix is predominantly smooth brome, a situation that best reflects the Type III DD scenario, the lower probability of remaining in the patch ($\alpha = 0.83$), slower rate of diffusion in the matrix (D_0 is 0.767 in mudflat and 0.197 in brome) or shorter step lengths, decreases the likelihood of returning to the patch. A larger patch is needed to support a viable planthopper population. The minimum patch size for all three DD scenarios when the matrix is brome is estimated to be 2.10 m^2 using (11) and 2.33 m^2 using (43). Qualitatively, these model results are in accord with experimental predictions regarding minimum patch size (Cronin and Haynes 2004; Cronin 2007). In those experiments, planthoppers in cordgrass patches 0.66 m^2 in size persisted for five generations when the matrix was 100% mudflat but went extinct when the matrix was 100% brome.

A sensitivity analysis using both (11) and (43) for the case where the matrix was 100% mudflat or 100% brome (see Table 12) revealed that the intrinsic growth rate, followed by the probability of remaining in the patch are the two most important parameters in predicting minimum patch size. Here, we only focused on the Type I DD scenario for the mudflat and the Type III DD scenario for the brome as they best reflect the behavior of these planthoppers under the respective matrix conditions. If the true value of the intrinsic growth rate was known, the variance of the predictions of persistence could be reduced by 52–82% for each matrix type. Similarly, if the true value of α was known, it would reduce the variance by 5–24% for each matrix type. For all parameters, the importance of direct effects considerably outweighed those of interactive effects. This analysis indicates that for this planthopper, more accurate minimum patch size estimates can be achieved by using more resources in empirical studies to estimate intrinsic growth rate and probability of remaining in the patch than the remaining parameters.

Table 12 Sensitivity analysis for planthopper minimum population size for the cases using (11) and (43) where the matrix was 100% mudflat and the Type I DD scenario was used and 100% brome and the Type III DD scenario was used, respectively

	r	D	S_0	D_0	α
<i>Type I AND Type III DD using (11)</i>					
Main effect (%)	52.0	6.1	10.1	0.0	23.6
Interaction effect (%)	6.9	1.8	2.7	0.0	5.3
Total effect (%)	58.8	7.9	12.8	0.0	29.0
<i>Type I DD using (43)</i>					
Main effect (%)	81.5	5.7	0.3	0.0	6.3
Interaction effect	9.4	7.2	0.7	0.0	5.2
Total effect (%)	90.9	12.9	1.0	0.0	11.5
<i>Type III DD using (43)</i>					
Main effect (%)	73.5	4.5	0.3	0.0	5.3
Interaction effect (%)	15.6	11.6	0.5	0.0	4.6
Total effect (%)	89.1	16.1	0.8	0.0	9.9

7 Summary and Conclusions

As the spatial heterogeneity of the landscape is increased through habitat fragmentation, the quality and structure of the matrix has the potential to alter movement behavior of the species inhabiting the landscape, ultimately changing the ability of the remnant patches to support viable and persistent populations [e.g., Tschamtkke et al. (2002), Schooley and Wiens (2004), Haynes and Cronin (2006), Cronin and Reeve (2005), Reeve and Cronin (2010)]. Even though ecologists are able to gather a wealth of movement data at a small scale, they often struggle to explain observations of population density at the patch or landscape level. This work helps to formalize the connection between small-scale movement and patch-level predictions of persistence through a mechanistic model based on the reaction–diffusion framework. The model is capable of incorporating essential information about edge-mediated effects such as patch preference, movement behavior, and matrix-induced mortality at the patch/matrix interface. This framework extends the model, and in particular the boundary condition used to model the patch/matrix interface, developed in Maciel and Lutscher (2013) to a more general one-, two-, or three-dimensional patch with a smooth boundary. Numerical exploration of the accuracy of the framework in several convex patch geometries indicates that if the steady-state density distribution in the matrix is well approximated by a certain exponential decay, then the framework will yield fairly accurate estimates of patch persistence for the parameter of interest. Finally, this framework allows for the consequences of four different patch–matrix interface scenarios considered in Maciel and Lutscher (2013), Cantrell and Cosner (2007) to be studied. As we illustrate with a well-studied planthopper species living in a highly fragmented landscape, the model’s explicit parameters can be estimated through empirical studies and used to predict critical population metrics like persistence and provide an estimate of minimum patch size under the context of changing landscape structure. Additionally, the model framework permits an explicit analysis and comparison of the implications of these four different patch/matrix interface scenario assumptions.

Our first conclusion is that the observed discrepancies in predictions of minimum patch size between the different interface scenarios discussed in Maciel and Lutscher (2013) are now confirmed for more general one-, two-, or three-dimensional patches with sufficiently smooth boundary. Under any interface scenario, exposure to an unsuitable matrix was shown to induce a minimum patch size required for the model to predict persistence. With respect to the probability that an organism remained in the patch upon reaching the patch/matrix interface or the death rate in the matrix, the behavior of the minimum patch size was consistent across interface scenarios. Minimum patch size decreased as the probability of staying in the patch increased [see Cronin (2007)] and increased as the death rate in the matrix increased. However, with regard to the matrix diffusion rate, the model showed starkly different predictions across interface scenarios. As suggested in Maciel and Lutscher (2013), these results show that whether organisms move faster or slower in a patch versus the matrix critically affects population patterns and needs to be considered carefully. In particular, the same species could inhabit patches of the exact same size and shape but surrounded by a matrix structure that induces fast movement in the matrix surrounding the first patch and slow movement in the second. If the organism maintained the same movement step sizes but altered its movement probability in the patch versus the matrix (Type II DD), then the organism may be unable to colonize the second patch, while able to colonize the first. If the organism instead altered its movement step sizes in the patch versus the matrix but maintained the same movement probability in both (Type I DD), then colonization of both patches would be independent of the matrix diffusion rate. In a sense, the global nature of our results shows that the mechanism behind these discrepancies is invariant with respect to (reasonable) domain geometry. Overall, the models suggest that minimum patch size for population persistence is critically dependent on these aspects of animal movement and boundary behavior [see also Cantrell et al. (2001), Ovaskainen and Cornell (2003), Reeve and Cronin (2010), Maciel and Lutscher (2013)]. Interestingly, of the many methods used to estimate minimum patch size for real species, they are rarely mechanistic and do not consider these important dispersal parameters [McCoy and Mushinsky (2007); but see Reeve and Cronin (2010)].

The utility of this model was demonstrated with a planthopper (*P. crocea*) whose dispersal behavior has been studied extensively by one of the authors. The model not only provided predictions about minimum patch size for a pure mudflat and pure brome matrix but also provided predictions for minimum patch size for any proportion of the two matrix types. These models demonstrated that minimum patch size in this species grew with increasing percentage of brome in the matrix. Qualitatively, the model results were also in accord with experimental predictions regarding minimum patch size. Interestingly, as smooth brome has invaded tall-grass prairies of the Great Plains, cordgrass habitat has disappeared, resulting in reduced size of cordgrass patches (Dillemuth et al. 2009). The high extinction rate of planthopper populations in small brome-embedded patches could be explained by our model prediction that for planthoppers to persist, brome-embedded patches need to be at least 2.103 m^2 .

Admittedly, the data needed to parameterize this model are challenging to obtain and rarely available, but it is becoming increasingly obvious that these behaviors are important to understanding the spatial and temporal dynamics of species in heteroge-

neous landscapes (Ovaskainen 2004; Cronin and Reeve 2005, 2014). Our sensitivity analysis revealed that most critical parameters for obtaining precise predictions about species persistence and minimum patch size for persistence are the intrinsic growth rate and the probability that the organisms will remain in the patch upon encountering the edge. This finding underscores the importance of boundary behavior and the need for careful experimental studies that quantify it. Experimental studies like Ries and Debinski (2001), Goodwin and Fahrig (2002), Haynes and Cronin (2006), Reeve et al. (2008) provide a template for collecting these important field data.

The second conclusion of this work is that care must be taken in studying the dynamics of a reaction diffusion model containing a form of a Robin boundary condition when choosing the parameter of interest, i.e., determining the dynamics of the model as a single parameter is varied and the remaining parameters held fixed. Such a model's boundary condition can take on different forms depending on the parameter of interest and interface scenario assumption. In addition to establishing the existence of a minimum patch size required for predictions of persistence by the model, an analog was also established for intrinsic growth rate by considering the intrinsic growth rate as the parameter of interest. In this case, the existence of such a minimum growth rate appeared under each of the interface scenarios. The boundary condition for patch size as the parameter of interest was consistent across interface scenarios, as well as the boundary condition for intrinsic growth rate. However, when exploring the dynamics of the model with patch diffusion rate as the parameter of interest, the boundary condition was completely different between continuous density/Type I DD/Type III DD and Type II DD. The mathematics literature contains vast amount of works detailing the dynamics of population models similar to the ones studied here. Typically, these models are assumed to have already been scaled to a dimensionless form. As an axillary conclusion of this work, we assert that results given in the mathematical literature should be carefully viewed in light of the difference that patch/matrix interface assumptions made on the scaling of the model. In other words, a scaled, dimensionless reaction diffusion model contains implicit assumptions regarding the patch/matrix interface.

In conclusion, we have made an attempt to tackle extension of the patch/matrix interface scenarios in Maciel and Lutscher (2013) to patches in two and three dimensions. This framework is built upon an assumption regarding the stationary state of population density in the matrix. For one-dimensional patches, the model under this assumption will exactly capture the mechanistically correct model results (e.g., minimum patch size predictions) of Maciel and Lutscher (2013), and based upon our numerical results, we conjecture that it will provide a reasonable approximation in simply connected, convex patches in higher dimensions. Analysis of our model shows confirmation of many results from previous authors including those in the now famous Skellam (1951), further confirming its validity as a framework for exploring the effects of patch/matrix interface scenarios on population persistence in higher-dimensional patches. The utility of this framework is demonstrated via application to a well-studied planthopper species (*Prokelisia crocea*) living in a highly fragmented landscape. Using experimentally derived data from various sources to parameterize the model, we show that, qualitatively, the model results are in accord with experimental predictions regarding minimum patch size of *P. crocea*. Finally, our results seem to indicate that great care

should be taken by both mathematicians and ecologists in their mathematical analysis of nondimensional models and their parameter dependence.

Acknowledgements The authors would like to thank the three anonymous reviewers whose suggestions greatly improved this manuscript.

Appendix A Sensitivity Analysis Methodology

In this subsection, we will briefly describe the sensitivity analysis methodology which was applied to the model. Following Saltelli et al. (2008, 2010), we generate a ten-dimensional list of quasi-random parameter values, i.e., tuples of the form $(x_1^0, x_2^0, x_3^0, x_4^0, x_5^0, x_1^1, x_2^1, x_3^1, x_4^1, x_5^1)$, of length N based on the Sobol quasi-random sequence. Two matrices **A** and **B** of size $(N, 5)$ are then constructed using the first half of the N tuples for the rows of **A** and the remainder for the rows of **B**. Thus, a row of the matrix **A** or **B** will contain values for these five parameters. A third matrix $\mathbf{A}_B^{s_1, s_2, \dots, s_i}$ is then constructed using all the columns of **A** except columns s_1, s_2, \dots, s_i are taken from the matrix **B**, where $s_1, s_2, \dots, s_i, i \in \{1, 2, 3, 4, 5\}$. For example, \mathbf{A}_B^2 is matrix **A** where the second column is taken from **B** and $\mathbf{A}_B^{2,3}$ is matrix **A** where the second and third columns are taken from **B**.

We now define the function $h(\mathbf{x})$ as the output of the model (either minimum patch size, minimum intrinsic growth rate, or maximum patch diffusion rate) given the five parameters $\mathbf{x} = (x_1, x_2, x_3, x_4, x_5)$ and a fixed patch geometry in Ω_0 . We then compute the model output for all input values in the three matrices, **A**, **B**, and $\mathbf{A}_B^{s_1, s_2, \dots, s_i}$ giving the N -dimensional vectors $h(\mathbf{A}), h(\mathbf{B}),$ and $h(\mathbf{A}_B^{s_1, s_2, \dots, s_i})$. Using these matrices, we can generate an estimate of the first-order interaction (main effect) of x_i

$$S_{x_i} = \frac{\frac{1}{N} \sum_{m=1}^N [h(\mathbf{A}_m) (h((\mathbf{A}_B^i)_m) - h(\mathbf{B}_m))] }{\frac{1}{2^{N-1}} \sum_{m=1}^N [(h(\mathbf{A}_m) - h_0)^2 + (h(\mathbf{B}_m) - h_0)^2]}$$

and total effect index of x_i

$$S_{T_{x_i}} = \frac{\frac{1}{N} \sum_{m=1}^N (h(\mathbf{B}_m) - h((\mathbf{A}_B^i)_m))^2}{\frac{1}{2^{N-1}} \sum_{m=1}^N [(h(\mathbf{A}_m) - h_0)^2 + (h(\mathbf{B}_j) - h_0)^2]},$$

where $i \in \{1, 2, 3, 4, 5\}, h_0 = \frac{1}{2^{N-1}} \sum_{m=1}^N [h(\mathbf{A}_m) + h(\mathbf{B}_m)]$, and $\mathbf{A}_m, \mathbf{B}_m$ represent the m -th rows of the matrices **A** and **B**, respectively.

Since the modeling framework is presented in a general form in order to accommodate as many species as possible, no species-specific parameter ranges were chosen. Instead, all the parameters' ranges were set to $[0.01, 100]$, with the exception of the probability of remaining in the patch upon reaching the patch/matrix interface, α , whose range was chosen as $[0.01, 0.99]$. An algorithm was implemented in Mathematica (Wolfram Research Inc., version 11.3), (1) to compute estimates of these sensitivity indices. In the algorithm, N was initially set to 250 and the main effect indices were calculated iteratively as N was incremented by 250 each time. This process continued until the norm of the difference between the vectors of successive main

effect indices was within our predetermined goal of 0.0005, indicating convergence of the estimated indices to the actual ones. The final value of N was then used to compute estimates for the total effect index. A simple geometry was chosen for Ω_0 in that it was only considered as a disk in two spatial dimensions. As changes in patch geometry affect the predictions of the model, an extension of our results could include performing a sensitivity analysis on the model with patch geometry counted and varied as a parameter in the analysis. This is, however, out of the scope of this work.

Appendix B Statement and Proof of Lemma 1

Lemma 1 *Let $\lambda_1(\Omega_0, \beta)$ be the principal eigenvalue of (14) with corresponding eigenfunction, ϕ , which is chosen such that $\phi > 0$; $x \in \overline{\Omega_0}$ and $\|\phi\|_\infty = 1$. Then, we have the following:*

- (a) $\lambda_1(\Omega_0, 0) = 0$, $\lambda_1(\Omega, \beta)$ is a strictly increasing function of β , and $\lambda_1(\Omega_0, \beta) \rightarrow \lambda_1^0(\Omega_0)$ as $\beta \rightarrow \infty$, where $\lambda_1^0(\Omega_0)$ is the principal eigenvalue of Laplace’s equation with Dirichlet boundary conditions ($u = 0$; $x \in \partial\Omega_0$).
- (b) $\lambda_1(\Omega_0, \beta)$ is a differentiable function of β .
- (c) $\lambda_1(\Omega_0, \beta)$ is a concave function of β .

The proof of (a) and (b) is standard, see Cantrell and Cosner (2003). The proof of (c) is as follows. For brevity, we denote $\lambda_1(\beta) = \lambda_1(\Omega_0, \beta)$. We begin by differentiating (14) with respect to β yielding

$$\begin{aligned}
 -\Delta\phi'(\beta) &= \lambda_1'(\beta)\phi(\beta) + \lambda_1(\beta)\phi'(\beta); \quad x \in \Omega_0 \\
 \frac{\partial\phi'(\beta)}{\partial\eta} + \phi(\beta) + \beta\phi'(\beta) &= 0; \quad x \in \partial\Omega_0,
 \end{aligned}
 \tag{26}$$

where $'$ denotes differentiation with respect to β . Next, we calculate $\lambda_1'(\beta)$ for any $\beta > 0$. By Green’s second identity, we have:

$$\begin{aligned}
 \int_{\Omega_0} [(-\Delta\phi(\beta))\phi'(\beta) + \phi(\beta)(\Delta\phi'(\beta))] dx &= \int_{\partial\Omega_0} \frac{-\partial\phi(\beta)}{\partial\eta} \phi'(\beta) \\
 &+ \phi(\beta) \frac{\partial\phi'(\beta)}{\partial\eta} ds
 \end{aligned}
 \tag{27}$$

But, we also have that

$$\begin{aligned}
 &\int_{\Omega_0} [(-\Delta\phi(\beta))\phi'(\beta) + \phi(\beta)(\Delta\phi'(\beta))] dx \\
 &= \int_{\Omega_0} \lambda_1(\beta)\phi(\beta)\phi'(\beta) - \phi(\beta)\lambda_1'(\beta)\phi(\beta) - \lambda_1(\beta)\phi(\beta)\phi'(\beta) dx \\
 &= -\lambda_1'(\beta) \int_{\Omega_0} [\phi^2(\beta)] dx
 \end{aligned}
 \tag{28}$$

and

$$\begin{aligned} & \int_{\partial\Omega_0} \frac{-\partial\phi(\beta)}{\partial\eta} \phi'(\beta) + \phi(\beta) \frac{\partial\phi'(\beta)}{\partial\eta} ds \\ &= \int_{\partial\Omega_0} \left[\beta\phi(\beta)\phi'(\beta) - \phi^2(\beta) - \beta\phi(\beta)\phi'(\beta) \right] ds \\ &= - \int_{\partial\Omega_0} \phi^2(\beta) ds. \end{aligned} \tag{29}$$

Combining (28) and (29) gives,

$$\lambda'_1(\beta) = \frac{\int_{\partial\Omega_0} \phi^2(\beta) ds}{\int_{\Omega_0} \phi^2(\beta) dx} > 0; \beta \geq 0. \tag{30}$$

Now, by Green’s first identity and (14), we have

$$\begin{aligned} \int_{\Omega_0} [(-\Delta\phi(\beta)) \phi(\beta)] dx &= \int_{\Omega_0} |\nabla\phi(\beta)|^2 dx - \int_{\partial\Omega_0} \frac{\partial\phi(\beta)}{\partial\eta} \phi(\beta) ds \\ &= \int_{\Omega_0} |\nabla\phi(\beta)|^2 dx + \beta \int_{\partial\Omega_0} \phi^2(\beta) ds. \end{aligned} \tag{31}$$

Also, from (14) we have that

$$\int_{\Omega_0} [(-\Delta\phi(\beta)) \phi(\beta)] dx = \lambda_1(\beta) \int_{\Omega_0} \phi^2(\beta) dx. \tag{32}$$

Combining (31) and (32) and solving for $\int_{\partial\Omega_0} \phi^2(\beta) ds$ yields

$$\int_{\partial\Omega_0} \phi^2(\beta) ds = \frac{1}{\beta} \lambda_1(\beta) \int_{\Omega_0} \phi^2(\beta) dx - \frac{1}{\beta} \int_{\Omega_0} |\nabla\phi(\beta)|^2 dx. \tag{33}$$

Thus, if we combine (30) with (33), then we have

$$\lambda'_1(\beta) = \frac{1}{\beta} \lambda_1(\beta) - \frac{1}{\beta \int_{\Omega_0} \phi^2(\beta) dx} \int_{\Omega_0} |\nabla\phi(\beta)|^2 dx; \beta > 0. \tag{34}$$

Hence,

$$\lambda'_1(\beta) \leq \frac{\lambda_1(\beta)}{\beta}; \beta > 0, \tag{35}$$

which proves that $\lambda_1(\beta)$ is a concave function for $\beta > 0$. □

Appendix C Special Case of a Disk-Shaped Patch in Two Dimensions

In this subsection, we present a derivation and mathematical analysis of a mechanistically correct model (at least in the sense of steady states and their stability properties) in the special case of a disk-shaped patch in two dimensions with radius $\ell > 0$ and patch population density denoted by $v(t, \rho)$, namely

$$\begin{aligned}
 v_t &= D \left(v_{\rho\rho} + \frac{1}{\rho} v_\rho \right) + rvf(v); \quad t > 0, \rho \in (0, \ell) \\
 v(0, \rho) &= v_0(\rho); \quad \rho \in (0, \ell) \\
 v_\rho &= 0; \quad t > 0, \rho = 0 \\
 Dv_\rho + \frac{\sqrt{S_0 D_0}}{\kappa} H \left(\sqrt{\frac{S_0}{D_0}} \ell \right) v &= 0; \quad t > 0, \rho = \ell
 \end{aligned} \tag{36}$$

where

$$H(s) = \frac{K_1(s)}{K_0(s)}, \tag{37}$$

and K_0, K_1 are modified Bessel functions of the second kind with all the parameters defined as in Sect. 2.

C.1 Derivation

Following the modeling setup as in Sect. 2, we assume that the patch is disk-shaped with radius $\ell > 0$, i.e., $\Omega = \{x \in \mathbb{R}^2 \mid |x| < \ell\}$, with $u(t, x)$ representing the density in Ω , and the matrix is the region exterior to Ω , i.e., $\Omega_e = \{x \in \mathbb{R}^2 \mid |x| \geq \ell\}$, with $w(t, x)$ representing the density in the matrix. Assuming a growth law similar to (2) in the matrix and the same patch/matrix interface assumptions as in Sect. 2.1, we have the following system to describe the population dynamics of an organism in this patch/matrix system:

$$\begin{aligned}
 u_t &= D\Delta u + ruf(u); \quad t > 0, x \in \Omega \\
 w_t &= D_0\Delta w - S_0w; \quad t > 0, x \in \Omega_e \\
 u(0, x) &= u_0(x); \quad x \in \Omega \\
 w(0, x) &= 0; \quad x \in \Omega_e \\
 D \frac{\partial u}{\partial \eta} &= D_0 \frac{\partial w}{\partial \eta_0}; \quad t > 0, |x| = \ell \\
 u(t, x) &= \kappa w(t, x); \quad t > 0, |x| = \ell \\
 w(t, x) &\rightarrow 0; \quad t > 0, \text{ as } |x| \rightarrow \infty.
 \end{aligned} \tag{38}$$

Making use of the rotational symmetry of the patch/matrix system, we convert the system $(u(t, x), w(t, x))$ to $(v(t, \rho), \omega(t, \rho))$ yielding

$$\begin{aligned}
 v_t &= D \left(v_{\rho\rho} + \frac{1}{\rho} v_\rho \right) + rvf(v); \quad t > 0, \rho \in (0, \ell) \\
 \omega_t &= D_0 \left(\omega_\rho + \frac{1}{\rho} \omega_\rho \right) - S_0\omega; \quad t > 0, \rho \in (\ell, \infty) \\
 v(0, \rho) &= v_0(\rho); \quad \rho \in (0, \ell) \\
 \omega(0, \rho) &= 0; \quad \rho \in (\ell, \infty) \\
 Dv_\rho &= D_0\omega_\rho; \quad t > 0, \rho = \ell \\
 v(t, \ell) &= \kappa\omega(t, \ell); \quad t > 0 \\
 v_\rho &= 0; \quad t > 0, \rho = 0 \\
 \omega(t, \rho) &\rightarrow 0; \quad t > 0, \text{ as } \rho \rightarrow \infty.
 \end{aligned}
 \tag{39}$$

We now make the assumption that the population density is at a stationary state in the matrix which must be of the form $\omega(\rho) = C_1 K_0 \left(\sqrt{\frac{S_0}{D_0}} \rho \right)$ for $\rho \geq \ell$ [see, for example, Skellam (1951)]. Notice that $\omega'(\rho) = -C_1 \sqrt{\frac{S_0}{D_0}} K_1 \left(\sqrt{\frac{S_0}{D_0}} \rho \right)$. Thus, applying the interface conditions at $\rho = \ell$ in (39) to this solution yields

$$Dv_\rho + \frac{\sqrt{S_0 D_0}}{\kappa} \frac{K_1 \left(\sqrt{\frac{S_0}{D_0}} \ell \right)}{K_0 \left(\sqrt{\frac{S_0}{D_0}} \ell \right)} v = 0; \quad t > 0, \rho = \ell.
 \tag{40}$$

With this Robin boundary condition, it is now possible to consider the problem only inside the patch via the dynamical problem, (36). Although the nonstationary solutions of (36) are not equivalent to those of the original patch/matrix system in (38), the argument given in Potapov and Lewis (2004) ensures that the stationary solutions of (36) and their stability properties are equivalent to the ones in the original system.

Applying the scaling

$$\tilde{\rho} = \frac{\rho}{\ell} \quad \& \quad \tilde{t} = rt,
 \tag{41}$$

and dropping the tilde, (36) becomes:

$$\begin{aligned}
 v_t &= \frac{1}{\lambda} \left(v_{\rho\rho} + \frac{1}{\rho} v_\rho \right) + vf(v); \quad t > 0, \rho \in (0, 1) \\
 v(0, \rho) &= v_0(\rho); \quad \rho \in (0, 1) \\
 v_\rho &= 0; \quad t > 0, \rho = 0 \\
 v_\rho + \frac{\ell\sqrt{S_0 D_0}}{\kappa D} H \left(\sqrt{\frac{S_0}{D_0}} \ell \right) v &= 0; \quad t > 0, \rho = 1
 \end{aligned}
 \tag{42}$$

where $\lambda = \frac{r\ell^2}{D}$ is unitless. In Table 13, we enumerate the different possibilities for the boundary condition of (42) as the different scenarios and patch attributes are changed. We then write the multiparameter model (42) in such a way as to ensure that the original parameters are split into three unitless composite parameters, namely λ , γ_1 , and γ_2 , in such a way that the parameter in question (r , D , or ℓ) occurs only in λ . This process gives several different forms of the boundary condition in (42) as listed in Table 13. We note that under the assumption of $D = D_0$ in CD and Type III DD interface scenarios, the boundary conditions for these two cases are different than that of Type I DD. Recall that the CD scenario can be considered as a special case of Type III DD in which $\alpha = \frac{1}{2}$.

As in Sect. 2, all twelve parameters of interest and interface condition pairs can be treated mathematically via study of the multiparameter problem:

$$\begin{aligned}
 v_t &= \frac{1}{\lambda} \left(v_{\rho\rho} + \frac{1}{\rho} v_\rho \right) + vf(v); \quad t > 0, \quad \rho \in (0, 1) \\
 v(0, \rho) &= v_0(\rho); \quad \rho \in (0, 1) \\
 v_\rho &= 0; \quad t > 0, \quad \rho = 0 \\
 v_\rho + \lambda^{\mu_1} \gamma_1 H(\lambda^{\mu_2} \gamma_2) v &= 0; \quad t > 0, \quad \rho = 1
 \end{aligned}
 \tag{43}$$

where $\mu_1, \mu_2 = 0, \frac{1}{2}$ and the meaning of the unitless parameters γ_1, γ_2 will depend on the parameter of interest and interface type.

C.2 Mathematical Analysis of (43)

As in Sect. 3, the dynamics of (43) are almost completely determined by its steady states, i.e., solutions of

$$\begin{aligned}
 - \left(v'' + \frac{1}{\rho} v_\rho \right) &= \lambda vf(v); \quad \rho \in (0, 1) \\
 v'(0) &= 0 \\
 v'(1) + \lambda^{\mu_1} \gamma_1 H(\lambda^{\mu_2} \gamma_2) v(1) &= 0.
 \end{aligned}
 \tag{44}$$

Given a solution of (44), v , its local stability properties can be determined by examining the sign of the principal eigenvalue, $\sigma_1 = \sigma_1(\Omega_0, \lambda, \gamma_1, \gamma_2, \mu_1, \mu_2, v)$, of the linearized eigenvalue problem associated with (44):

$$\begin{aligned}
 - \left(\phi'' + \frac{1}{\rho} \phi' \right) - \lambda [f(v) + vf'(v)] \phi &= \sigma \phi; \quad \rho \in (0, 1) \\
 \phi'(0) &= 0 \\
 \phi'(1) + \lambda^{\mu_1} \gamma_1 H(\lambda^{\mu_2} \gamma_2) \phi(1) &= 0
 \end{aligned}
 \tag{45}$$

with $\Omega_0 = (0, 1)$ and corresponding eigenfunction, ϕ , which can be chosen such that $\phi > 0$; $x \in [0, 1]$ and $\|\phi\|_\infty = 1$.

Table 13 Boundary condition possibilities for (42)

Parameter of interest	Type I DD	Type II DD	Type III DD
r : intrinsic growth rate	$\kappa = \frac{\alpha}{1-\alpha} \sqrt{\frac{D_0}{D}}$	$\kappa = \frac{\alpha}{1-\alpha} \frac{D_0}{D}$	$\kappa = \frac{\alpha}{1-\alpha}$
	$v_\rho + \gamma_1 H(\gamma_2)v = 0; \rho = 1$	$v_\rho + \gamma_1 H(\gamma_2)v = 0; \rho = 1$	$v_\rho + \gamma_1 H(\gamma_2)v = 0; \rho = 1$
	$\gamma_1 = \frac{1-\alpha}{\alpha} \sqrt{\frac{S_0}{D}} \ell$	$\gamma_1 = \frac{1-\alpha}{\alpha} \sqrt{\frac{S_0}{D_0}} \ell$	$\gamma_1 = \frac{1-\alpha}{\alpha} \sqrt{\frac{S_0}{D}} \ell$
	$\gamma_2 = \sqrt{\frac{S_0}{D_0}} \ell$	$\gamma_2 = \sqrt{\frac{S_0}{D_0}} \ell$	$\gamma_2 = \sqrt{\frac{S_0}{D}} \ell$
D : patch diffusion rate	$v_\rho + \sqrt{\lambda} \gamma_1 H(\gamma_2)v = 0; \rho = 1$	$v_\rho + \gamma_1 H(\gamma_2)v = 0; \rho = 1$	$v_\rho + \sqrt{\lambda} \gamma_1 H(\sqrt{\lambda} \gamma_2)v = 0; \rho = 1$
	$\gamma_1 = \frac{1-\alpha}{\alpha} \sqrt{\frac{S_0}{r}}$	$\gamma_1 = \frac{1-\alpha}{\alpha} \sqrt{\frac{S_0}{D_0}} \ell$	$\gamma_1 = \frac{1-\alpha}{\alpha} \sqrt{\frac{S_0}{r}}$
	$\gamma_2 = \sqrt{\frac{S_0}{D_0}} \ell$	$\gamma_2 = \sqrt{\frac{S_0}{D_0}} \ell$	$\gamma_2 = \sqrt{\frac{S_0}{r}}$
	$v_\rho + \sqrt{\lambda} \gamma_1 H(\sqrt{\lambda} \gamma_2)v = 0; \rho = 1$	$v_\rho + \sqrt{\lambda} \gamma_1 H(\sqrt{\lambda} \gamma_2)v = 0; \rho = 1$	$v_\rho + \sqrt{\lambda} \gamma_1 H(\sqrt{\lambda} \gamma_2)v = 0; \rho = 1$
ℓ : patch size	$\gamma_1 = \frac{1-\alpha}{\alpha} \sqrt{\frac{S_0}{r}}$	$\gamma_1 = \frac{1-\alpha}{\alpha} \sqrt{\frac{S_0 D}{r D_0}}$	$\gamma_1 = \frac{1-\alpha}{\alpha} \sqrt{\frac{S_0}{r}}$
	$\gamma_2 = \sqrt{\frac{S_0}{D_0}} \ell$	$\gamma_2 = \sqrt{\frac{S_0}{D_0}} \ell$	$\gamma_2 = \sqrt{\frac{S_0}{r}}$
	$v_\rho + \sqrt{\lambda} \gamma_1 H(\sqrt{\lambda} \gamma_2)v = 0; \rho = 1$	$v_\rho + \sqrt{\lambda} \gamma_1 H(\sqrt{\lambda} \gamma_2)v = 0; \rho = 1$	$v_\rho + \sqrt{\lambda} \gamma_1 H(\sqrt{\lambda} \gamma_2)v = 0; \rho = 1$
	$\gamma_2 = \sqrt{\frac{S_0 D}{r D_0}}$	$\gamma_2 = \sqrt{\frac{S_0 D}{r D_0}}$	$\gamma_2 = \sqrt{\frac{S_0}{r}}$

Note that the continuous density scenario is a special case of Type III DD with $\alpha = \frac{1}{2}$, where DD denotes discontinuous density as described in Table 2

As in Sect. 3, model predictions of persistence can be determined by studying the stability of the trivial steady state, $v \equiv 0$, via consideration of the sign of $\sigma_1(\Omega_0, \lambda, \gamma_1, \gamma_2, \mu_1, \mu_2, 0)$. In the case of a reaction term satisfying the logistic-type assumptions, (F1) and (F2), Theorem 1 allows an exact description of the global dynamics of (43) based solely on the sign of $\sigma_1(\Omega_0, \lambda, \gamma_1, \gamma_2, \mu_1, \mu_2, v)$. In the following analysis, we will explicitly describe the relationship between a given parameter of interest (r, D , or ℓ) and the persistence of the population under each of the four interface scenarios given in Table 1 via comparison of the linearized eigenvalue problem for the trivial steady state, (45), with the eigenvalue problem (14). Uniqueness of the principal eigenvalue again implies that:

$$\begin{aligned} \lambda_1(\Omega_0, \beta) &= \sigma_1(\Omega_0, \lambda, \gamma_1, \gamma_2, \mu_1, \mu_2, 0) + \lambda & (46) \\ \beta &= \lambda^{\mu_1} \gamma_1 H(\lambda^{\mu_2} \gamma_2). & (47) \end{aligned}$$

In the case of $\mu_2 = 0$ and $\mu_1 = 0$ or $\frac{1}{2}$, the mathematical analysis of (43) exactly follows that of Sect. 4 with $\gamma = \gamma_1 H(\gamma_2)$. The only remaining case is $\mu_2 = \mu_1 = \frac{1}{2}$, for which (46) & (47) become:

$$\sigma_1(\Omega_0, \lambda, \gamma_1, \gamma_2, 0.5, 0.5, 0) = \lambda_1(\Omega_0, \sqrt{\lambda} \gamma_1 H(\sqrt{\lambda} \gamma_2)) - \lambda \tag{48}$$

Theorem 4 connects the sign of $\sigma_1(\Omega_0, \lambda, \gamma_1, \gamma_2, 0.5, 0.5, 0)$ to ranges of parameter space for λ, γ_1 , and γ_2 .

Theorem 4 *Let $\gamma_1, \gamma_2 > 0$. Then, we have the following:*

(a) *there exists a $\lambda_3^*(\Omega_0, \gamma_1, \gamma_2) > 0$ such that*

- (1) *if $\lambda \leq \lambda_3^*(\Omega_0, \gamma_1, \gamma_2)$, then $\sigma_1(\Omega_0, \lambda, \gamma_1, \gamma_2, 0.5, 0.5, 0) \geq 0$*
- (2) *if $\lambda > \lambda_3^*(\Omega_0, \gamma_1, \gamma_2)$, then $\sigma_1(\Omega_0, \lambda, \gamma_1, \gamma_2, 0.5, 0.5, 0) < 0$.*

(b) *$\lambda_3^*(\Omega_0, 0, \gamma_2) = 0$ and $\lambda_3^*(\Omega_0, \gamma_1, \gamma_2) \rightarrow \lambda_1^0(\Omega_0)$ as $\gamma_1 \rightarrow \infty$ for all $\gamma_2 > 0$.*

A proof of Theorem 4 is given in Sect. C.4.

C.3 Results

Interpreting λ as being proportional to the intrinsic growth rate r , we can employ Corollary 1 to arrive at a minimum intrinsic growth rate given in (23) with $\gamma = \gamma_1 H(\gamma_2)$, namely

$$r^{**}(\Omega_0, \gamma_1, \gamma_2) = r^*(\Omega_0, \gamma_1 H(\gamma_2)). \tag{49}$$

Similarly, interpreting λ as being proportional to the patch diffusion rate D , we can employ Corollary 2 to arrive at a maximum patch diffusion rate, namely

$$D^{**}(\Omega_0, \gamma_1, \gamma_2) = \begin{cases} D^*(\Omega_0, \gamma_1 H(\gamma_2)); & \text{Type I DD} \\ D^*(\Omega_0, \gamma_1 H(\gamma_2)); & \text{Type II DD} \\ \frac{r \ell^2}{\lambda_3^*(\Omega_0, \gamma_1, \gamma_2)}; & \text{CD or Type III DD} \end{cases} \tag{50}$$

Finally, interpreting λ as being proportional to the patch size ℓ , we present a corresponding minimum patch size required for a prediction of persistence for the theoretical population given a fixed patch diffusion rate and patch intrinsic growth rate:

$$\ell^{**}(\Omega_0, \gamma_1, \gamma_2) = \sqrt{\frac{D}{r} \lambda_3^*(\Omega_0, \gamma_1, \gamma_2)}. \tag{51}$$

Using (48) and Theorem 4 yields the following result detailing the connection between the patch size and predictions of persistence from the model.

Corollary 4 *Let $\gamma_1, \gamma_2 > 0$ be defined as in Table 13 according to the interface scenario assumed. Then, we have the following:*

- (a) *if $\ell > \ell^{**}(\Omega_0, \gamma_1, \gamma_2)$, then (43) has a unique positive equilibrium, v , that is a global attractor for nonnegative nontrivial solutions of (43);*
- (b) *if $\ell \leq \ell^{**}(\Omega_0, \gamma_1, \gamma_2)$, then $v \equiv 0$ is a global attractor for nonnegative nontrivial solutions of (43).*

C.4 Proof of Theorem 4

Before we present a proof for Theorem 4, we first present and prove a useful lemma, namely

Lemma 2 *Let $g(s) = \sqrt{s}\gamma_1 H(\sqrt{s}\gamma_2)$. Then, for all $\gamma_1, \gamma_2 > 0$ we have the following:*

- (a) *$\lambda_1(\Omega_0, g(\lambda))$ is a strictly increasing function of λ for all $\lambda > 0$*
- (b) *$\lambda_1(\Omega_0, g(\lambda)) \rightarrow 0$ as $\lambda \rightarrow 0^+$ and $\lambda_1(\Omega_0, g(\lambda)) \rightarrow \lambda_1^0(\Omega_0)$ as $\lambda \rightarrow \infty$*
- (c) *$\lambda_1(\Omega_0, g(\lambda))$ is a concave function of λ for all $\lambda > 0$.*

Proof of Lemma 2 To prove (a), we first note that $k_1(s) > k_0(s) > 1; s > 0$ [see Yang and Chu (2016)]. It is then easy to see that

$$\frac{d}{d\lambda} [\lambda_1(\Omega_0, g(\lambda))] = \lambda_1'(\Omega_0, g(\lambda)) \frac{\gamma_1 \gamma_2 (k_1^2(\sqrt{\lambda}\gamma_2) - k_0^2(\sqrt{\lambda}\gamma_2))}{2k_0^2(\sqrt{\lambda}\gamma_2)} > 0$$

since $\lambda_1(\Omega_0, \beta)$ is strictly increasing in β (see Lemma 1). To show (b), we first consider the Taylor series for k_0 and k_1 both centered at $s = 0$, namely

$$k_1(s) = \frac{1}{s} + O(s) \tag{52}$$

$$k_0(s) = -\Gamma + \ln(2) - \ln(s) + O(s) \tag{53}$$

where Γ is Euler’s constant. Thus,

$$\lim_{\lambda \rightarrow 0^+} \lambda_1(\Omega_0, g(\lambda)) = \lambda_1 \left(\Omega_0, \lim_{\lambda \rightarrow 0^+} \gamma_1 \sqrt{\lambda} \frac{k_1(\sqrt{\lambda}\gamma_2)}{k_0(\sqrt{\lambda}\gamma_2)} \right) \\ \lambda_1 \left(\Omega_0, \lim_{\lambda \rightarrow 0^+} \gamma_1 \sqrt{\lambda} \frac{\frac{1}{\sqrt{\lambda}\gamma_2} + O(\sqrt{\lambda}\gamma_2)}{-\Gamma + \ln(2) - \ln(\sqrt{\lambda}\gamma_2) + O(\sqrt{\lambda}\gamma_2)} \right). \tag{54}$$

Making the change of variables $t = \sqrt{\lambda}\gamma_2$, (54) becomes

$$\lim_{\lambda \rightarrow 0^+} \lambda_1(\Omega_0, g(\lambda)) = \lambda_1 \left(\Omega_0, \lim_{t \rightarrow 0^+} \frac{\gamma_1}{\gamma_2} \frac{1+O(t^2)}{-\Gamma + \ln(2) - \ln(t) + O(t)} \right) = 0 \tag{55}$$

since by Lemma 1 $\lambda_1(\Omega_0, \beta) \rightarrow 0$ as $\beta \rightarrow 0^+$. Also, from Yang and Chu (2016), $H(\sqrt{\lambda}\gamma_2) \rightarrow 1$ as $\lambda \rightarrow \infty$ for fixed $\gamma_2 > 0$ and thus $g(\lambda) \rightarrow \infty$ as $\lambda \rightarrow \infty$. This fact and Lemma 1 give that $\lambda_1(\Omega_0, g(\lambda)) \rightarrow \lambda_1^0(\Omega_0)$ as $\lambda \rightarrow \infty$.

Finally, to show (c), we note that since Lemma 1 gives that $\lambda_1(\Omega_0, \beta)$ is concave in β and $\lambda_1(\Omega_0, \beta)$ is strictly increasing in β it suffices to show that $g(s)$ is concave in s , or equivalently that

$$g'(\lambda) = \frac{\gamma_1\gamma_2}{2} \left(\frac{k_1(\sqrt{\lambda}\gamma_2)}{k_0(\sqrt{\lambda}\gamma_2)} - 1 \right) \leq \frac{\gamma_1 k_1(\sqrt{\lambda}\gamma_2)}{\sqrt{\lambda} k_0(\sqrt{\lambda}\gamma_2)} = \frac{g(\lambda)}{\lambda}; \lambda > 0. \tag{56}$$

It is easy to see that (56) will hold as long as

$$\frac{1}{\sqrt{\lambda}} (\sqrt{\lambda}\gamma_2 - 2) \frac{k_1(\sqrt{\lambda}\gamma_2)}{k_0(\sqrt{\lambda}\gamma_2)} - \gamma_2 \leq 0; \lambda > 0. \tag{57}$$

Clearly, (57) will hold if $\sqrt{\lambda}\gamma_2 - 2 \leq 0$. Thus, assume $\sqrt{\lambda}\gamma_2 - 2 > 0$. Using the fact that $\frac{k_1(\sqrt{\lambda}\gamma_2)}{k_0(\sqrt{\lambda}\gamma_2)} < 1 + \frac{1}{2\sqrt{\lambda}\gamma_2}$ for all $\lambda, \gamma_2 > 0$ [see Yang and Chu (2016)], (57) becomes

$$\frac{1}{\sqrt{\lambda}} (\sqrt{\lambda}\gamma_2 - 2) \frac{k_1(\sqrt{\lambda}\gamma_2)}{k_0(\sqrt{\lambda}\gamma_2)} - \gamma_2 < \frac{1}{\sqrt{\lambda}} (\sqrt{\lambda}\gamma_2 - 2) \frac{2\sqrt{\lambda}\gamma_2 + 1}{2\sqrt{\lambda}\gamma_2} - \gamma_2 \\ = \frac{1}{2\gamma_2\lambda} (2\lambda\gamma_2^2 - 3\sqrt{\lambda}\gamma_2 - 2) - \gamma_2 \\ = \frac{1}{2\gamma_2\lambda} (-3\sqrt{\lambda}\gamma_2 - 2) < 0. \tag{58}$$

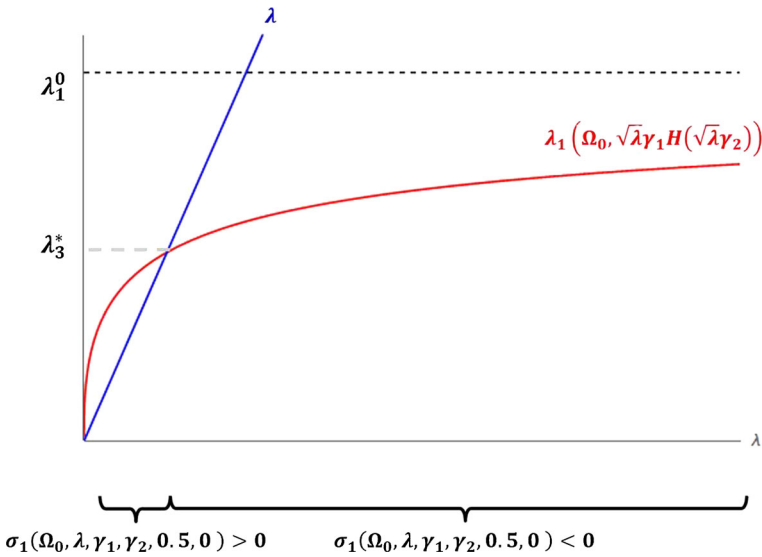


Fig. 3 Illustration of Theorem (Color figure online) 4

Hence, $g(\lambda)$ is a concave function of λ for $\lambda > 0$, which implies $\lambda_1(\mathcal{D}_0, g(\lambda))$ is a concave function of λ for all $\lambda > 0$. □

Now we present a proof of Theorem 4.

Proof of Theorem 4 Define $g(s) = \sqrt{s}\gamma_1 H(\sqrt{s}\gamma_2)$. and let $\gamma_1, \gamma_2 > 0$. From Lemma 2, we have that $\lambda_1(\mathcal{D}_0, g(0)) = 0$, $\lambda_1(\mathcal{D}_0, g(\lambda))$ is a strictly increasing and concave function of λ for $\lambda > 0$, and $\lambda_1(\mathcal{D}_0, g(\lambda)) \rightarrow \lambda_1^0(\mathcal{D}_0)$ as $\lambda \rightarrow \infty$. Also, from the proof of Lemma 2 and the fact that we can choose $\phi > 0$; $x \in \overline{\mathcal{D}_0}$, we have that $\lambda_1'(\mathcal{D}_0, g(0)) > 0$. It is now clear that $\lambda_1(\mathcal{D}_0, g(\lambda)) - \lambda > 0$ for $\lambda > 0$ and small enough. But, since $\lambda_1(\mathcal{D}_0, g(\lambda))$ is concave, strictly increasing, and bounded in λ there exists a unique $\lambda_3^*(\mathcal{D}_0, \gamma_1, \gamma_2) > 0$ such that $\sigma_1(\mathcal{D}_0, \lambda, \gamma_1, \gamma_2, 0.5, 0.5, 0) = \lambda_1(\mathcal{D}_0, g(\lambda)) - \lambda \geq 0$ for $\lambda \in [0, \lambda_3^*(\mathcal{D}_0, \gamma_1, \gamma_2)]$ and $\sigma_1(\mathcal{D}_0, \lambda, \gamma_1, \gamma_2, 0.5, 0.5, 0) = \lambda_1(\mathcal{D}_0, g(\lambda)) - \lambda < 0$ for $\lambda > \lambda_3^*(\mathcal{D}_0, \gamma_1, \gamma_2)$, proving part (a) (see Fig. 3). Part (b) is clear from Lemma 2 and the previous argument. □

References

Allen CR, Pearlstone LG, Kitchens WM (2001) Modeling viable mammal populations in gap analyses. *Biol Conserv* 99(2):135–144. [https://doi.org/10.1016/S0006-3207\(00\)00084-7](https://doi.org/10.1016/S0006-3207(00)00084-7)

Cantrell RS, Cosner C (1998) Skew brownian motion: a model for diffusion with interfaces. In: *Proceedings of the international conference on mathematical models in the medical and health sciences*. Vanderbilt University Press, Nashville, Tennessee, USA, pp 74–78

Cantrell RS, Cosner C (1999) Diffusion models for population dynamics incorporating individual behavior at boundaries: applications to refuge design. *Theor Popul Biol* 55(2):189–207. <https://doi.org/10.1006/tubi.1998.1397>

- Cantrell RS, Cosner C (2003) Spatial ecology via reaction–diffusion equations. mathematical and computational biology. Wiley, Hoboken
- Cantrell RS, Cosner C (2007) Density dependent behavior at habitat boundaries and the Allee effect. *Bull Math Biol* 69:2339–2360. <https://doi.org/10.1007/s11538-007-9222-0>
- Cantrell RS, Cosner C, Fagan WF (1998) Competitive reversals inside ecological reserves: the role of external habitat degradation. *J Math Biol* 37(6):491–533. <https://doi.org/10.1007/s002850050139>
- Cantrell RS, Cosner C, Fagan WF (2001) How predator incursions affect critical patch size: the role of the functional response. *Am Nat* 158(4):368–375. <https://doi.org/10.1086/321989>
- Cronin JT (2003) Movement and spatial population structure of a prairie planthopper. *Ecology* 84(5):1179–1188
- Cronin JT (2007) From population sources to sieves: the matrix alters host–parasitoid source–sink structure. *Ecology* 88(12):2966–2976
- Cronin JT (2009) Habitat edges, within-patch dispersion of hosts, and parasitoid oviposition behavior. *Ecology* 90(1):196–207. <https://doi.org/10.1890/08-0208.1>
- Cronin JT, Haynes KJ (2004) An invasive plant promotes unstable host–parasitoid patch dynamics. *Ecology* 85(10):2772–2782 URL ISI:000224844700017
- Cronin JT, Reeve JD (2005) Hostparasitoid spatial ecology: a plea for a landscape-level synthesis. *Proc R Soc B Biol Sci* 272(1578):2225–2235. <https://doi.org/10.1098/rspb.2005.3286>
- Cronin JT, Reeve JD (2014) An integrative approach to understanding host–parasitoid population dynamics in real landscapes. *J Appl Basic Ecol* 15:101–113
- Cronin JT, Haynes KJ, Dillemoth F (2004) Spider effects on planthopper mortality, dispersal, and spatial population dynamics. *Ecology* 85(8):2134–2143. <https://doi.org/10.1890/03-0591>
- Dillemoth FP, Rietschier EA, Cronin JT (2009) Patch dynamics of a native grass in relation to the spread of invasive smooth brome (*Bromus inermis*). *Biol Invasions* 11(6):1381–1391. <https://doi.org/10.1007/s10530-008-9346-7>
- Ewers RM, Didham RK, Pearse WD, Lefebvre V, Rosa IMD, Carreiras JMB, Lucas RM, Reuman DC (2013) Using landscape history to predict biodiversity patterns in fragmented landscapes. *Ecol Lett* 16(10):1221–1233. <https://doi.org/10.1111/ele.12160>
- Fagan WF, Cantrell RS, Cosner C (1999) How habitat edges change species interactions. *Am Nat* 153(2):165–182. <https://doi.org/10.1086/303162>
- Fahrig L (2001) How much habitat is enough? *Biol Conserv* 100(1):65–74. [https://doi.org/10.1016/S0006-3207\(00\)00208-1](https://doi.org/10.1016/S0006-3207(00)00208-1)
- Ferretti F, Saltelli A, Tarantola S (2016) Trends in sensitivity analysis practice in the last decade. *Sci Total Environ* 568:666–670. <https://doi.org/10.1016/j.scitotenv.2016.02.133>
- Goodwin BJ, Fahrig L (2002) Effect of landscape structure on the movement behaviour of a specialized goldenrod beetle, *Trirhabda borealis*. *Can J Zool* 80(1):24–35. <https://doi.org/10.1139/z01-196>
- Haynes KJ, Cronin JT (2003) Matrix composition affects the spatial ecology of a prairie planthopper. *Ecology* 84(11):2856–2866. <https://doi.org/10.1890/02-0611>
- Haynes KJ, Cronin JT (2006) Interpatch movement and edge effects: the role of behavioral responses to the landscape matrix. *Oikos* 113(1):43–54
- Heilman GE, Strittholt JR, Slosser NC, Dellasala DA (2002) Forest fragmentation of the conterminous united states: assessing forest intactness through road density and spatial characteristics: forest fragmentation can be measured and monitored in a powerful new way by combining remote sensing, geographic information systems, and analytical software. *BioScience* 52(5):411–422. [https://doi.org/10.1641/0006-3568\(2002\)052\[0411:FFOTCU\]2.0.CO;2](https://doi.org/10.1641/0006-3568(2002)052[0411:FFOTCU]2.0.CO;2)
- Holmes EE, Lewis MA, Banks RRV (1994) Partial differential equations in ecology: spatial interactions and population dynamics. *Ecology* 75(1):17–29
- Ludwig D, Aronson DG, Weinberger HF (1979) Spatial patterning of the spruce budworm. *J Math Biol* 8:217–258
- Maciel GA, Lutscher F (2013) How individual movement response to habitat edges affects population persistence and spatial spread. *Am Nat* 182(1):42–52. <https://doi.org/10.1086/670661>
- McCoy ED, Mushinsky HR (2007) Estimates of minimum patch size depend on the method of estimation and the condition of the habitat. *Ecology* 88(6):1401–1407. <https://doi.org/10.1890/06-1188>
- Ohman K, Eriksson LO (1998) The core area concept in forming contiguous areas for long-term forest planning. *Can J For Res* 28(7):1032–1039. <https://doi.org/10.1139/x98-076>
- Okubo A (1980) Diffusion and ecological problems: mathematical models, biomathematics, vol 10. Springer, Berlin

- Ovaskainen O (2004) Habitat-specific movement parameters estimated using markrecapture data and a diffusion model. *Ecology* 85(1):242–257. <https://doi.org/10.1890/02-0706>
- Ovaskainen O, Cornell SJ (2003) Biased movement at a boundary and conditional occupancy times for diffusion processes. *J Appl Probab* 40(3):557–580. <https://doi.org/10.2307/3215936>
- Potapov AB, Lewis MA (2004) Climate and competition: the effect of moving range boundaries on habitat invasibility. *Bull Math Biol* 66:975–1008
- Reeve JD, Cronin JT (2010) Edge behaviour in a minute parasitic wasp. *J Anim Ecol* 79(2):483–490. <https://doi.org/10.1111/j.1365-2656.2009.01640.x>
- Reeve JD, Cronin JT, Haynes KJ (2008) Diffusion models for animals in complex landscapes: incorporating heterogeneity among substrates, individuals and edge behaviours. *J Anim Ecol* 77(5):898–904
- Ries L, Debinski DM (2001) Butterfly responses to habitat edges in the highly fragmented prairies of Central Iowa. *J Anim Ecol* 70(5):840–852. <https://doi.org/10.1046/j.0021-8790.2001.00546.x>
- Ries L, Fletcher Robert J, Battin JJ, Sisk TD (2004) Ecological responses to habitat edges: mechanisms, models, and variability explained. *Annu Rev Ecol Evolut Syst* 35(1):491–522. <https://doi.org/10.1146/annurev.ecolsys.35.1.12202.130148>
- Saltelli A, Tarantola S, Campolongo F, Ratto M (2004) Sensitivity analysis in practice: a guide to assessing scientific models. Wiley, Hoboken
- Saltelli A, Ratto M, Andres T, Campolongo F, Cariboni J, Gatelli D, Saisana M, Tarantola S (2008) Global sensitivity analysis: the primer. Wiley, Hoboken
- Saltelli A, Annoni P, Azzini I, Campolongo F, Ratto M, Tarantola S (2010) Variance based sensitivity analysis of model output. Design and estimator for the total sensitivity index. *Comput Phys Commun* 181(2):259–270. <https://doi.org/10.1016/j.cpc.2009.09.018>
- Schooley RL, Wiens JA (2004) Movements of cactus bugs: patch transfers, matrix resistance, and edge permeability. *Landsc Ecol* 19(7):801–810. <https://doi.org/10.1007/s10980-005-0093-2>
- Sibly RM, Barker D, Denham MC, Hone J, Pagel M (2005) On the regulation of populations of mammals, birds, fish, and insects. *Science* 309(5734):607–610
- Skellam JG (1951) Random dispersal in theoretical populations. *Biometrika* 38:196–218
- Solomon M, Van Jaarsveld AS, Biggs HC, Knight MH (2003) Conservation targets for viable species assemblages? *Biodivers Conserv* 12(12):2435–2441. <https://doi.org/10.1023/a:1025805731366>
- Tscharntke T, Steffan-Dewenter I, Kruess A, Thies C (2002) Contribution of small habitat fragments to conservation of insect communities of grassland-c-ropland landscapes. *Ecol Appl* 12(2):354–363. <https://doi.org/10.2307/3060947>
- Turchin P (1998) Quantitative analysis of movement: measuring and modeling population redistribution in animals and plants. Sinauer Associates Sunderland, Sunderland
- Uchida K, Ushimaru A (2014) Biodiversity declines due to abandonment and intensification of agricultural lands: patterns and mechanisms. *Ecol Monogr* 84(4):637–658. <https://doi.org/10.1890/13-2170.1>
- Yang ZH, Chu YM (2016) On approximating the modified bessel function of the first kind and Toader-Qi mean. *J Inequalities Appl* 1:40. <https://doi.org/10.1186/s13660-016-0988-1>

Publisher's Note Springer Nature remains neutral with regard to jurisdictional claims in published maps and institutional affiliations.

Affiliations

James T. Cronin¹ · Jerome Goddard II²  · Ratnasingham Shivaji³

✉ Jerome Goddard II
jgoddard@aum.edu

James T. Cronin
jcronin@lsu.edu

Ratnasingham Shivaji
r_shivaj@uncg.edu

- ¹ Department of Biological Sciences, Louisiana State University, Baton Rouge, LA 70803, USA
- ² Department of Mathematics and Computer Science, Auburn University Montgomery, Montgomery, AL 36124, USA
- ³ Department of Mathematics and Statistics, University of North Carolina Greensboro, Greensboro, NC 27402, USA